Redox Biology 13 (2017) 370–385

Contents lists available at ScienceDirect

Redox Biology

journal homepage: www.elsevier.com/locate/redox

Research paper

The SGLT2 inhibitor empagliflozin improves the primary diabetic complications in ZDF rats

Sebastian Steven[a,b,1], Matthias Oelze[a,1], Alina Hanf[a,1], Swenja Kröller-Schön[a], Fatemeh Kashani[a], Siyer Roohani[a], Philipp Welschof[a], Maximilian Kopp[a], Ute Gödtel-Armbrust[c], Ning Xia[c], Huige Li[c,f], Eberhard Schulz[a], Karl J. Lackner[d], Leszek Wojnowski[c], Serge P. Bottari[e], Philip Wenzel[a,b,f], Eric Mayoux[g], Thomas Münzel[a,f], Andreas Daiber[a,f,*]

[a] Center for Cardiology, Cardiology I – Laboratory of Molecular Cardiology, Medical Center of the Johannes Gutenberg University, Mainz, Germany
[b] Center for Thrombosis and Hemostasis, Medical Center of the Johannes Gutenberg University, Mainz, Germany, Medical Center of the Johannes Gutenberg University, Mainz, Germany
[c] Department of Pharmacology, Medical Center of the Johannes Gutenberg University, Mainz, Germany
[d] Institute of Clinical Chemistry and Laboratory Medicine, Medical Center of the Johannes Gutenberg University, Mainz, Germany
[e] Institute for Advanced Biosciences, INSERM U1209 – CNRS UMR 5309, Grenoble-Alps University and Institute for Biology and Pathology, CHU, Grenoble, France
[f] German Center for Cardiovascular Research (DZHK), Partner Site Rhine-Main, Mainz, Germany
[g] Boehringer Ingelheim Pharma GmbH & Co. KG, Biberach, Germany

ARTICLE INFO

Keywords:
SGLT2 inhibitor
Zucker diabetic fatty rats
Diabetes
Oxidative stress
Endothelial dysfunction
Low-grade inflammation
AGE/RAGE signaling
β-cell content

ABSTRACT

Hyperglycemia associated with inflammation and oxidative stress is a major cause of vascular dysfunction and cardiovascular disease in diabetes. Recent data reports that a selective sodium-glucose co-transporter 2 inhibitor (SGLT2i), empagliflozin (Jardiance®), ameliorates glucotoxicity via excretion of excess glucose in urine (glucosuria) and significantly improves cardiovascular mortality in type 2 diabetes mellitus (T2DM). The overarching hypothesis is that hyperglycemia and glucotoxicity are upstream of all other complications seen in diabetes. The aim of this study was to investigate effects of empagliflozin on glucotoxicity, β-cell function, inflammation, oxidative stress and endothelial dysfunction in Zucker diabetic fatty (ZDF) rats. Male ZDF rats were used as a model of T2DM (35 diabetic ZDF-Lepr$^{fa/fa}$ and 16 ZDF-Lepr$^{+/+}$ controls). Empagliflozin (10 and 30 mg/kg/d) was administered via drinking water for 6 weeks. Treatment with empagliflozin restored glycemic control. Empagliflozin improved endothelial function (thoracic aorta) and reduced oxidative stress in the aorta and in blood of diabetic rats. Inflammation and glucotoxicity (AGE/RAGE signaling) were epigenetically prevented by SGLT2i treatment (ChIP). Linear regression analysis revealed a significant inverse correlation of endothelial function with HbA1c, whereas leukocyte-dependent oxidative burst and C-reactive protein (CRP) were positively correlated with HbA1c. Viability of hyperglycemic endothelial cells was pleiotropically improved by SGLT2i. Empagliflozin reduces glucotoxicity and thereby prevents the development of endothelial dysfunction, reduces oxidative stress and exhibits anti-inflammatory effects in ZDF rats, despite persisting hyperlipidemia and hyperinsulinemia. Our preclinical observations provide insights into the mechanisms by which empagliflozin reduces cardiovascular mortality in humans (EMPA-REG trial).

Abbreviations used: ACh, acetylcholine; AGE, advanced glycation end products; ALDH-2, mitochondrial aldehyde dehydrogenase; CCL-2, see MCP-1; ChIP, chromatin immunoprecipitation; COX2, cyclooxygenase-2; CRP, C-reactive protein; DHE, dihydroethidine; DHFR, dihydrofolate reductase; DMSO, dimethylsulfoxide; DPP-4, dipeptidyl peptidase-4; ECL, enhanced chemiluminescence; ecSOD, extracellular superoxide dismutase; eNOS, endothelial ˙NO synthase (type 3); FPS-ZM1, RAGE inhibitor; GTN, glyceryl trinitrate (nitroglycerin); H2K9me2, histone3 lysine9 dimethylation; HbA1c, glycohemoglobin; HG, hyperglycemia; HO-1, heme oxygenase-1; IFN-γ, interferon-γ; IL-6, interleukin-6; ICAM-1, intercellular adhesion molecule-1; L-012, 8-amino-5-chloro-7-phenylpyrido[3,4-*d*]pyridazine-1,4-(2H,3H)dione sodium salt; MCP-1, monocyte-chemoattractant-protein-1; NG, normoglycemia; Nox, catalytic subunit of NADPH oxidase; PKC, protein kinase C; qRT-PCR, quantitative reverse transcription polymerase chain reaction; RAGE, receptor for AGE; ROS, reactive oxygen species; sGC, soluable guanylyl cyclase; SGLT2, sodium-glucose co-transporter-2; SGLT2i, SGLT2 inhibitor; TNF-α, tumor necrosis factor-α; ZDF, Zucker diabetic fatty (rat)

* Corresponding author at: Universitätsmedizin der Johannes Gutenberg-Universität Mainz, Zentrum für Kardiologie, Kardiologie I – Labor für Molekulare Kardiologie, Geb. 605 – Raum 3.262, Langenbeckstr. 1, 55131 Mainz, Germany.
E-mail address: andreas.daiber@bioredox.com (A. Daiber).
[1] The authors contributed equally to this study and should therefore all be considered as first author.

http://dx.doi.org/10.1016/j.redox.2017.06.009
Received 29 May 2017; Received in revised form 20 June 2017; Accepted 21 June 2017
Available online 22 June 2017

1. Introduction

Hyperglycemia is a major risk factor for the development of cardiovascular disease and cardiovascular mortality [1,2]. Diabetic complications are associated with oxidative stress and uncoupling of endothelial nitric oxide synthase (eNOS, type 3) (reviewed in [3]). Both parameters are considered important pathological mechanisms in the development of vascular dysfunction in diabetic animals [4–6] and patients [7,8]. Another major cause for vascular damage under hyperglycemic conditions is based on direct toxic effects of high glucose levels via the formation of advanced glycation end products (AGE) and activation of their specific receptors (RAGE) [9,10]. Of note, there is a vital cross-talk between oxidative stress and AGE/RAGE components [11–13] leading to increased inflammation [14–16], accounting at least in part for the vascular dysfunction in the diabetic state.

The sodium-glucose co-transporter 2 (SGLT2) is responsible for the renal reabsorption of > 90% of the glucose from primary urine [17]. Inhibitors of SGLT2 (SGLT2i) are new therapeutic agents in the treatment of type 2 diabetes (T2DM). These agents increase urinary excretion of glucose, and thereby prevent hyperglycemic episodes in diabetic animals and individuals as well as the resulting glucotoxicity [18,19]. SGLT2i act independently of insulin secretion and are therefore not affected by deteriorating β-cell function and desensitization to insulin signaling (as observed with increasing age) [20]. Empagliflozin, a potent and highly selective SGLT2i, was approved in the United States of America [21] and European Union (European Medicines Agency number: EMEA/H/C/002677) for the treatment of T2DM. The ability of SGLT2i to prevent hyperglycemia-induced damage is supported by recent large-scale clinical trials (EMPA-REG) where empagliflozin was the only modern anti-diabetic drug that reduced cardiovascular and overall mortality in T2DM patients at high cardiovascular risk [2,22]. So far, neither therapy with a dipeptidyl peptidase 4 inhibitor nor with a glucagon-like peptide-1 analogue showed a similar reduction in cardiovascular and overall mortality in T2DM patients with proven cardiovascular risk [23,24].

We recently described the anti-diabetic, antioxidant, anti-inflammatory and vasculo-protective effects of empagliflozin treatment in rats with streptozotocin-induced T1DM [18]. With the current study we sought to investigate the effects of empagliflozin on β-cell function, endothelial dysfunction, oxidative stress, AGE/RAGE signaling and inflammation in Zucker fatty diabetic rats, a well-established rat model of T2DM.

2. Materials and methods

2.1. Materials

The High-Capacity cDNA Reverse Transcription Kit was purchased from Applied Biosystems, Darmstadt, Germany. All oligonucleotides and dual labeled probes were purchased from MWG Biotech, Ebersberg, Germany. The Bradford reagent was obtained from BioRad, Munich, Germany. For isometric tension studies, nitroglycerin (GTN) was used from a Nitrolingual infusion solution (1 mg/ml) from G.Pohl-Boskamp (Hohenlockstedt, Germany). SGLT2-inhibitor (SGLT2i, empagliflozin) was a kind gift from Boehringer Ingelheim Pharma GmbH & Co KG (Biberach, Germany). L-012 (8-amino-5-chloro-7-phenylpyrido[3,4-*d*] pyridazine-1,4-(2H,3H)dione sodium salt) was purchased from Wako Pure Chemical Industries (Osaka, Japan). All other chemicals were of analytical grade and were obtained from Sigma-Aldrich, Fluka or Merck.

2.2. Animals and in vivo treatment

All animals were treated in accordance with the Guide for the Care and Use of Laboratory Animals as adopted by the U.S. National Institutes of Health and approval was granted by the Ethics Committee of the University Hospital Mainz and the Landesuntersuchungsamt Rheinland-Pfalz (Koblenz, Germany; permit number: 23 177-07/G 12-1-025). As a model of T2DM we used Zucker Diabetic Fatty (ZDF) rats. A total number of 35 diabetic ZDF rats (ZDF-Lepr$^{fa/fa}$) and respective 16 lean controls (ZDF-Lepr$^{+/+}$) were directly ordered from Charles River at an age of 16 ± 1 weeks. Rats were fed with Purina 5008 chow and divided into 4 treatment groups: lean control rats (ZDF-Lepr$^{+/+}$, Ctr), type 2 diabetic rats (ZDF-Lepr$^{fa/fa}$, ZDF), type 2 diabetic rats on SGLT2i low dose (10 mg/kg/d p.o.) or SGLT2i high dose (30 mg/kg/d p.o.) treatment via drinking water as described [18]. The two doses were calculated upon correction for the significant differences in pharmacokinetic parameters and metabolism between rodents and humans (e.g. half-life around 1–2 h in rodent and 10–12 h in man) and were previously reported to be efficient and to correspond to the equivalent active dose in humans [25–28]. After 6 weeks of treatment duration, animals were killed under isoflurane anesthesia by transection of the diaphragm and removal of the heart and thoracic aorta. Hyperglycemia as a marker for type 2 diabetes was assessed by glucose levels and glycosylated hemoglobin (HbA1c) in whole blood using the ACCU-CHEK Sensor system from Roche Diagnostics GmbH (Mannheim, Germany) and A1C Now^{+} system from Bayer HealthCare Diabetes Care (Basel, Switzerland), respectively.

2.3. Detection of serum cholesterol, triglyceride and interferon-γ levels

Serum cholesterol, triglyceride, high- and low-density lipoprotein (HDL, LDL) levels were analyzed in the Department of Clinical Chemistry, University Hospital Mainz, Germany, using the daily routine facilities for in-patient care.

2.4. Histological and immunohistochemical staining of aortic rings and pancreatic tissue

Sirius red staining for vascular fibrosis and trichrome staining was performed with paraffin-embedded samples of aortic tissue upon deparaffination [18]. Paraffin-embedded aortic samples were stained with primary antibodies against glucagon (pancreatic tissue: 1:4000, Abcam, UK), insulin (pancreatic tissue: 1:200, LifeSpan BioSciences, Seattle, USA), CD68 (aorta: 1:50, Cell signaling #4842, Leiden, The Netherlands), cyclooxygenase-2 (COX2) (aorta: 1:50, LifeSpan Biosciences, Inc, Seattle, USA) and 3-nitrotyrosine (3NT) (aorta: 1:200, Merck-Millipore, Darmstadt, Germany) [18]. For detection we used the LSAB 2 kit with biotinylated anti-mouse and –rat (DAKO, #K0609, Hamburg, Germany) or fluorescent labeling (Alexa Fluor 488 anti-rabbit glucagon, Alexa Fluor 555 anti-mouse insulin, Cell Signaling, Danvers, MA; DAPI 397–412 nm for nuclei, Carl Roth GmbH, Karlsruhe, Germany) at dilutions according to the manufacturer's instructions. For immunochemical detection streptavidin-HRP (DAKO) and then DAB reagent (peroxidase substrate Kit, Vector) were used as substrates. Quantification was performed using Image ProPlus 7.0 software (Media Cybernetics, Rockville, MD).

2.5. Detection of insulin, glucagon, leptin in aprotinin plasma or serum levels by RIA

Venous blood was transferred into plasma vials (BD Vacutainer K3E with 250 KIU aprotinin), left on ice for 30 min and centrifuged for 10 min at 2000 g. The supernatant (plasma) was stored at –80 °C. Quantitative measurement of insulin and glucagon levels was performed using a rat insulin (#SRI-13K) or glucagon (#GLK-32) RIA (Merck (Millipore), St. Charles, Missouri, USA) according to the manufacturer's instructions. Insulin levels were also measured in serum, which was generated without aprotinin and EDTA, using a rat insulin ELISA (DRG Instruments GmbH, Marburg, Germany). Leptin and adiponectin levels were determined using ELISA (Leptin Quantikine Elisa Mouse / Rat Immunoassay, Cat.-Nr. MOB00, R & D Systems, Wiesbaden,

Germany; Adiponectin (ADP) Elisa Mouse / Rat / Human, Cat.-Nr. MBS066180, MyBioSource, USA).

2.6. Isometric tension studies

Vasodilator responses to acetylcholine (ACh) were assessed with endothelium-intact isolated rat aortic rings mounted for isometric tension recordings in organ chambers as described previously [29] but here we used preconstriction with either noradrenalin (1 μM yielding approximately 80% of the maximal tone induced by KCl bolus) or the thromboxane receptor agonist U46,619 (1 μM yielding approximately 50% of the maximal tone induced by KCl bolus).

2.7. Detection of oxidative stress in whole blood, cardiac tissue and aorta

Whole blood leukocyte-dependent ROS formation was measured in fresh blood (in citrate tubes) upon stimulation with the fungal endotoxin zymosan A (50 μg/ml) and assessed with L-012 (100 μM) enhanced chemiluminescence (ECL) [30]. To investigate involvement of NADPH oxidase in ROS production, aortic rings were preincubated with the NADPH oxidase isoform 2 (Nox2) inhibitor VAS2870 and the intracellular calcium chelator BAPTA-AM [15,18]. Vascular ROS formation was determined using dihydroethidium (DHE, 1 μM)-dependent fluorescence microtopography in aortic cryo-sections as described [29,31]. To investigate the involvement of eNOS uncoupling in ROS production and endothelial dysfunction, aortic rings were preincubated with the NOS inhibitor L-NAME (0.5 mM) [29,31,32]. Adventitial ROS formation was measured by densitometric quantification of red fluorescence in a defined area within the adventitial tissue [33]. ROS-derived red fluorescence was detected using a Zeiss Axiovert 40 CFL microscope, Zeiss lenses and Axiocam MRm camera. Superoxide formation in heart membrane fractions was measured by an HPLC-based method to quantify ethidium and 2-hydroxyethidium yield from 50 μM DHE in the presence of NADPH (200 μM) as previously described [29].

2.8. eNOS immunoprecipitation, Western blot and dot blot analysis

Protein expression and modification was assessed by standard Western and dot blot analysis using established protocols [18,29]. Immunoprecipitation of eNOS was performed with M-280 sheep anti-mouse IgG coated beads from Invitrogen (Darmstadt, Germany) along with a monoclonal mouse eNOS (Biosciences, USA) antibody [33]. The precipitates were washed and transferred to gel and subjected to SDS-PAGE followed by a standard Western blot procedure using a monoclonal rabbit phospho-Thr495-eNOS antibody (P-eNOS^{Thr495}, 1:1000, Upstate Biotechnology, MA, USA). SDS-PAGE and Western blotting were performed as previously described [18,33] using monoclonal mouse α-actinin (1:10,000, Sigma-Aldrich, Munich, Germany) as a control for loading and transfer, monoclonal mouse NADPH oxidase isoform 2 (Nox2 or gp91^{phox}, 1:1000, BD Biosciences, USA), monoclonal mouse dihydrofolate reductase (DHFR, 1 μg/ml, Abnova Corp., Germany), monoclonal mouse GTP-cyclohydrolase-1 (GCH-1, 1 μg/ml, Abnova Corp., Germany), monoclonal mouse heme oxygenase-1 (HO-1) (4 μg/ml, Stressgen, San Diego, CA), polyclonal goat cGMP-dependent protein kinase (cGK-I, 1:200, Santa Cruz Biotechnologies, USA), vasodilator stimulated phosphoprotein (VASP) phosphorylated on serine239 (P-VASP^{Ser239}, clone 16C2, 1.5 μg/ml, Calbiochem, UK), polyclonal rabbit monocyte- chemoattractant-protein-1 (MCP-1 or CCL-2, 0.2 μg/ml, Serotec, UK), polyclonal rabbit receptor for advanced glycation end products (RAGE, 1:1000, Cell Signaling Technology, Danvers, MA), polyclonal mitochondrial aldehyde dehydrogenase (ALDH-2) (1:2000, provided by H. Weiner as previously characterized [34]). 4-Hydroxynonenal (HNE)-positive proteins and 3-nitrotyrosine (3NT)-positive proteins were assessed by dot blot analysis of aortic, renal or cardiac protein homogenates or serum samples, which was transferred to a Protran BA85 (0.45 μm) nitrocellulose membrane (Schleicher & Schuell, Dassel, Germany) by a Minifold I vacuum dot-blot system (Schleicher & Schuell, Dassel, Germany) [33]. A goat polyclonal HNE antibody (1:1000, Merck-Millipore, Darmstadt, Germany), a mouse monoclonal 3NT antibody (1:1000, Upstate Biotechnology, MA, USA) and a monoclonal mouse H3K9me2 antibody (1:1000, abcam #ab1220, UK) were used for dot blot analysis. Detection and quantification of all blots was performed by ECL with peroxidase conjugated anti–rabbit/mouse (1:10,000, Vector Lab., Burlingame, CA) and anti-goat (1:5000, Santa Cruz Biotechnologies, USA) secondary antibodies. Dot blot signals of serum samples were normalized to polyclonal rabbit transferrin (1:1000, Thermo Fisher, Waltham, USA) as the loading control. Densitometric quantification of antibody-specific bands was performed with a ChemiLux Imager (CsX-1400 M, Intas, Göttingen, Germany) and Gel-Pro Analyzer software (Media Cybernetics, Bethesda, MD).

2.9. Detection of serum methylglyoxal levels and liver ALDH-2 activity by HPLC-based quantification

Methylglyoxal serum levels were quantified by an HPLC-based method upon derivatization of the reactive aldehyde with 1,2-diaminobenzene as previously described [33]. The activity of ALDH-2 in isolated heart mitochondria was determined by measuring the conversion of 6-methoxy-2-naphthylaldehyde (Monal 62) to the fluorescent naphthoic acid product by an HPLC-based assay in the absence and presence of the specific ALDH-2 inhibitor daidzin [33].

2.10. Quantitative reverse transcription real-time PCR (qRT-PCR)

mRNA expression was analyzed with quantitative reverse transcription real-time PCR (qRT-PCR) as previously described [18,35]. Briefly, total RNA from rat aorta was isolated (RNeasy Fibrous Tissue Mini Kit; Qiagen, Hilden, Germany), and 50 ng of total RNA was used for real-time RT-PCR analysis with the QuantiTect Probe RT-PCR kit (Qiagen). TaqMan gene expression assays for inflammatory genes *interferon-γ* (*IFN-γ*), *cyclooxygenase-2* (*COX2*), *inducible NO synthase* (*NOS2*), *intercellular adhesion molecule-1 (ICAM-1)* and a marker of platelet and endothelial activation *P-selectin* (*SELP*) as well as the housekeeping gene *TATA box binding protein* (*TBP*) were purchased as probe-and-primer sets (Applied Biosystems, Foster City, CA). The comparative Ct method was used for relative mRNA quantification. Gene expression was normalized to the endogenous control, *TBP* mRNA, and the amount of target gene mRNA expression in each sample was expressed relative to the control.

2.11. Chromatin immunoprecipitation (ChIP)

Rat kidney samples were homogenized in liquid nitrogen and 50 mg kidney sample was used per ChIP experiment (modified from [36,37]). Samples were resuspended in PBS supplemented with protease inhibitors and single cells were obtained by filtering through a 100 μm mesh filter. The cells were then pelleted by low-speed centrifugation and lysed in cell lysis buffer containing protease inhibitors. DNA was fragmented using Micrococcal Nuclease to an average DNA fragment size of 300–400 bp. The nuclear membrane was broken using nuclear lysis buffer containing TritonX and SDS. 10 μg of DNA was used for each ChIP experiment and 1% (0.1 μg) DNA was retained as input control. Immunoprecipitations were performed by overnight incubation of the chromatin samples with protein G magnetic beads and 3 μg of the respective antibodies. Antibodies used were Anti-Histone H3 (trimethyl K9) antibody (abcam #ab8898) and Anti-Histone H3 (trimethyl K4) antibody (Millipore #07–473). After removal of the beads, the eluate was purified with the QIAQuick PCR Purification Kit (Qiagen #28104). Immunoprecipitated DNA was subjected to qPCR analysis using promoter-specific primers for *eNOS* [38], *NOS2*, *RAGE* and *IFNγ* (predicted from the UCSC genome browser: https://genome.ucsc.edu/). Chip data were calculated relative to input. Primer sequences for ChIP-qPCR

were: *eNOS*-forward CTGGCCCACACTCTTCAAGT, *eNOS*-reverse CCTAAGGAAAAGGCCAGGAC; *NOS2* forward CTGTCAGGGCCACAGCTTTA, *NOS2* reverse TCACCAAGGTGGCTGAGAAG; *RAGE*-forward GCTGGACCATGCTGCCTAAT, *RAGE*-reverse CATTTCCTTCAGCCCACCGA; *IFN*γ-forward GCCCAAGGAGTCGAAAGGAA, *IFN*γ-reverse AGATAGGTGGCGGGAGCTTA. The proper methodology of the ChIP procedure was validated by testing an always active gene (*GAPDH*, Simple CHIP Rat GAPDH Promoter Primers, Cell Signaling #7964) and an always inactive genomic region (gene desert, Rat Negative Control Primer Set 1, Active motif #71024) for activating (H3K4me3) and suppressing (H3K9me3) histone marks.

2.12. Cell culture

Human umbilical vein endothelial cells (HUVECs) were obtained from Academic Teaching Hospital in Frankfurt am Main/Höchst and Katholisches Klinikum Mainz St. Vincenz- und Elisabeth-Hospital. HUVECs were isolated by collagenase digestion as described [39], and cultured in endothelial growth medium (ECGM #C22110, Promocell) mixed 1:1 with M199 (#M4530, Sigma) containing 20% fetal calf serum (FCS, PAA), 0.5% penicillin / streptomycin and 1% L-glutamine at 37 °C and 5% CO_2. Then the cells were seeded into 6-well plates (0.6×10^6 cells/well) and grown until confluency was reached. On “day 0” the experiment was started by changing the medium to M199 only containing 10% fetal calf serum (FCS, PAA), 0.5% penicillin / streptomycin and 1% L-glutamine. Cells in one plate were cultured under normoglycemic conditions (5 mM glucose) and cells in 6 other plates were grown under hyperglycemic conditions (30 mM glucose). On “day 4” of normo- and hyperglycemic conditions the treatment with the SGLT2i empagliflozin, the dipeptidyl peptidase-4 inhibitor sitagliptin or the RAGE inhibitor FPS-ZM1 was started at concentrations of 1 or 10 μM (each stock in DMSO prepared for 1:1000 dilution) for another 3 days. The medium containing the different drugs or the solvent was changed daily. Pictures were taken on each day until “day 6″ and living cells were manually counted using the Cell B software (Olympus).

On “day 6“ the cells were stimulated with 1 μM acetylcholine for 30 min at 37 °C and the supernatant was subjected to HPLC analysis of nitrite. Medium with produced nitrite was mixed 1:1 with 1 M HCl containing 200 μM 2,3-diaminonaphthalene and incubated for 10 min at 37 °C. Under acidic conditions nitrite will form a highly fluorescent triazol product with 2,3-diaminonaphthalene. 50 μl of the supernatant were subjected to HPLC analysis. The system consisted of a control unit, two pumps, a mixer, detectors, a column oven, a degasser, an autosampler (AS-2057 plus) from Jasco (Groß-Umstadt, Germany), and a C_{18}-Nucleosil 100-3 (125 × 4) column from Macherey & Nagel (Düren, Germany). A high-pressure gradient was employed with solvent B (acetonitrile/water 90:10 v/v%) and solvent A (25 mM citrate buffer pH 2.2) as mobile phases with the following percentages of the organic solvent B: 0 min, 30%; 8 min, 65%; 8.5–9 min, 100%; and 9.5 min, 30%. The flow was 1 ml/min, and the triazol product was detected by its fluorescence (Ex. 375 nm/Em. 415 nm). Nitrite concentrations were quantified by external standards. The background nitrite signal of the culture medium was subtracted from the determined nitrite values.

2.13. Statistical analysis

Results are expressed as the means ± SEM. Two-way ANOVA (with Bonferroni's correction for comparison of multiple means) was used for comparisons of concentration-relaxation curves (Prism for Windows, version 6.05, GraphPad Software Inc.). One-way ANOVA (with Bonferroni's or Dunn's correction for comparison of multiple means), or, where appropriate, an equivalent non-parametric test (Dunn / Kruskal-Wallis multiple comparison) was used for comparisons of weight gain, blood glucose, HbA1c levels, other serum parameters, such as insulin, triglycerides and methylglyoxal levels, histological data, aortic ROS formation, protein and mRNA expression, cardiac and whole blood oxidative stress and mitochondrial ALDH-2 activity (SigmaStat for Windows, version 3.5, Systat Software Inc.). Correlations between fasting blood glucose, HbA1c and endothelial function, oxidative burst were analyzed by linear regression analysis (Prism for Windows, version 6.05, GraphPad Software Inc.). p values < 0.05 were considered as statistically significant. The number of replicates in the different assays may vary since not all animals were used in all assays and some values were excluded when they exceeded a deviation of 2xSD from the means.

3. Results

3.1. Metabolic syndrome-related parameters (Table 1)

Body weights and heart/body weight ratios were not significantly changed by SGLT2i treatment of ZDF rats. The kidney/body weight ratio was increased in ZDF rats and was not changed by SGLT2i treatment. Blood glucose was higher in all ZDF rats (more than 4-fold compared to the lean control rats) before SGLT2i treatment. Fasting blood glucose levels were decreased by approximately 40% after 6 weeks of SGLT2i treatment (both doses), with a trend for more pronounced anti-hyperglycemic effects of the higher dose SGLT2i treatment, but were still higher than blood glucose levels in lean control rats. The parameter for long-term glycemic conditions, HbA1c, was elevated in ZDF rats and was significantly decreased by both doses of empagliflozin. Insulin resistance, measured by the HOMA-IR index, was significantly increased in ZDF rats and was improved by the higher dose of empagliflozin. Accordingly, β-cell function as measured by the HOMA-beta index, was severely impaired in untreated ZDF rats and significantly improved by both doses of empagliflozin. ZDF rats had higher total cholesterol, HDL, LDL and triglyceride levels compared to lean control rats, which were not lowered by SGLT2i treatment. The severe hypercholesterolemia of all ZDF groups was also visible by the milky aspect of their serum (Fig. 1A). In accordance to the lack of effects of SGLT2i therapy on hypercholesterolemia and hyperlipidemia the levels of the adipokines leptin and adiponectin were not ameliorated by empagliflozin therapy.

Sirius red staining revealed neither thickening of the vascular wall nor increased fibrosis in the aorta of ZDF rats (not shown). The morphological changes (e.g. reduced β-cell mass and sclerosis of islets) in the pancreas as revealed by trichrome staining of the pancreas of untreated ZDF rats were normalized by the higher dose of SGLT2i (Fig. 1A). In accordance with this finding, immunohistochemical staining showed clear decreases of insulin and glucagon and only a few insulin-positive β-cells in the ZDF group as compared to the lean controls (Fig. 1A), implying that SGLT2i treatment may preserve insulin and glucagon content in islet cells, as confirmed by densitometric quantification of the immunohistochemical signals (Fig. 1B). Hyperinsulinemia in ZDF rats was not significantly improved by SGLT2i therapy as determined by insulin plasma values using RIA, whereas increased glucagon levels in plasma of ZDF rats were corrected by both SGLT2i doses (Table 1, from plasma with protease inhibitors).

3.2. Vascular parameters

The endothelial dysfunction (impaired acetylcholine [ACh]-dependent relaxation) in ZDF rats was partially prevented by both doses of SGLT2i (Fig. 2A-B). The modest increase in the expression of cGMP-dependent kinase in ZDF rats was reduced to control levels by SGLT2i treatment (Fig. 2C). Likewise, the phosphorylation of VASP at Ser239 (as a read-out of activation of the cGMP-dependent kinase) was decreased in ZDF rats, was normalized by the lower dose of SGLT2i treatment, and increased greater than in lean control rats with the higher dose of SGLT2i (Fig. 2C). As a consequence, the ratio of P-VASP/cGK-I was significantly decreased in ZDF rats and improved by SGLT2i treatment. A major determinant for the activity of the cGK-I is the

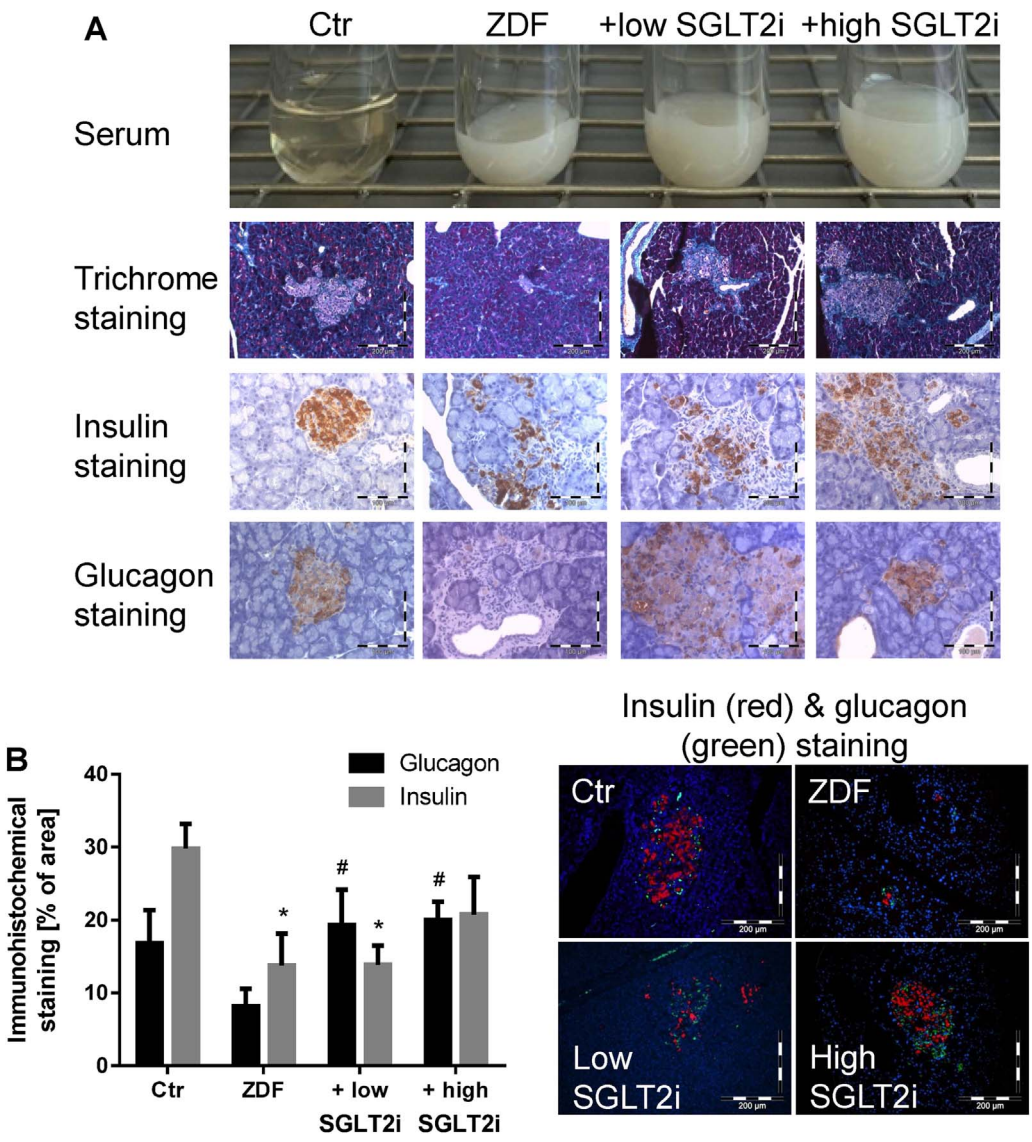

Fig. 1. Serum samples and immunohistochemical measurements in lean controls and ZDF rats with or without 6 weeks of SGLT2i (low and high dose) treatment. Representative picture of serum samples of all groups showing the milky color of ZDF serum due to hypercholesterolemia (**A**). Representative histological staining of pancreas with Goldner's trichrome for morphological changes of islets (**A**). Representative (immune)histochemical stainings of pancreatic tissue for insulin, glucagon and nuclei (**A**). Densitometric quantification of pancreatic insulin and glucagon formation and representative immunohistochemical stainings with the fluorescent antibodies and dyes (**B**). Representative data (means ± SEM) and pictures of at least 4 (**A**) or 7 (**B**) animals/group. *, $p < 0.05$ vs. control and #, $p < 0.05$ vs. ZDF group.

functional/coupling state of eNOS, which is largely determined by the availability of its cofactor tetrahydrobiopterin (BH_4) and its phosphorylation state. BH_4 levels are regulated by de novo synthesis by GTP-cyclohydrolase-1 (GCH-1) and by restoration of BH_4 from its oxidation product BH2 by dihydrofolate reductase (DHFR). GCH-1 protein expression was not changed among the groups but DHFR protein expression was increased by SGLT2i treatment (Fig. 2D). In addition, the inhibitory phosphorylation of eNOS at Thr495 (as characterized by Fleming and coworkers [40,41]) was diminished by SGLT2i treatment (Fig. 2D). The impact of oxidative stress on the $^{\bullet}NO$/cGMP signaling pathway and the role of the different components are illustrated in the scheme (Fig. 2E).

3.3. Oxidative stress parameters in whole blood, aorta, heart and kidney

The oxidative burst in whole blood in response to zymosan A was increased in ZDF rats and blunted in a dose-dependent fashion by SGLT2i treatment (Fig. 3A). The signal in the ZDF group was largely suppressed by the NADPH oxidase inhibitor VAS2870 (highest affinity for Nox2 isoform) and the intracellular calcium chelator BAPTA-AM, indicating the involvement of the phagocytic NADPH oxidase and $[Ca^{2+}]_i$ in this process (Fig. 3A). NADPH oxidase activity was increased in cardiac tissue of ZDF rats and inhibited by low dose SGLT2i treatment (Fig. 3B). Aortic reactive oxygen species formation was increased in aortic cryo-sections of ZDF rats and reduced by the highest dose of SGLT2i (Fig. 3C). An inhibitory effect of the eNOS inhibitor L-NAME on the reactive oxygen species signal in the endothelial cell layer is indicative of an uncoupled eNOS. SGLT2i treatment restored the L-NAME effect in ZDF rats to a pattern similar to the one observed in lean control rats (Fig. 3D). However, eNOS uncoupling could not be confirmed by eNOS S-glutathionylation (not shown). In line with increased cardiac oxidative stress, the activity of the redox-sensitive enzyme mitochondrial aldehyde dehydrogenase (ALDH-2) was decreased in heart mitochondria of ZDF rats and normalized with SGLT2i treatment (Fig. 3E). The specific ALDH-2 inhibitor daidzin showed a similar reduction of the overall ALDH activity as observed in ZDF rats, whereas the unspecific ALDH inhibitor benomyl reduced the measured activity to background levels. ALDH-2 expression was decreased by 18% in aortic tissue and normalized by SGLT2i treatment (not shown). The oxidative inactivation of ALDH-2 by reversible disulfide bridge formation and irreversible sulfonic acid generation are illustrated in the scheme (Fig. 3F).

Adventitial reactive oxygen species formation was increased in aortic cryo-sections of ZDF rats and reduced by SGLT2i therapies (Fig. 4A). Surrogate parameters for the burden of oxidative stress, 3NT- and HNE-positive proteins, were quantified by dot blot analysis in serum and both parameters were elevated in ZDF rats and almost normalized by SGLT2i treatments (Fig. 4B-C). 3NT-positive proteins were also quantified by dot blot analysis in renal tissue and were found

Table 1
Weight gain, and blood and serum parameters in controls and diabetic rats.

	In vivo treatment group			
Parameter[a]	Ctr	ZDF	ZDF + low SGLT2i	ZDF + high SGLT2i
Body weight [g]	386 ± 8 (n = 16)	367 ± 5 (n = 15)	382 ± 7 (n = 10)	395 ± 13 (n = 10)
Heart/body ratio (× 10^3)	3.5 ± 0.1 (n = 15)	3.7 ± 0.1 (n = 14)	3.7 ± 0.3 (n = 9)	3.4 ± 0.1 (n = 9)
Kidney/body ratio (× 10^3)	3.7 ± 0.1 (n = 15)	5.5 ± 0.1 (n = 14)*	5.4 ± 0.2 (n = 9)*	5.2 ± 0.2 (n = 9)*
Blood glucose [mg/dl], non-fast., prior SGLT2i	124 ± 4 (n = 16)	548 ± 13 (n = 15)*	518 ± 13 (n = 10)*	531 ± 21 (n = 10)*
Blood glucose [mg/dl], 6w SGLT2i, fasting	108 ± 5 (n = 15)	456 ± 23 (n = 14)*	230 ± 48(n = 9)*,#	157 ± 11 (n = 9)*,#
HbA1c [mmol/mol]	30 ± 1 (n = 16)	118 ± 4 (n = 15)*	71 ± 5 (n = 10)*,#	63 ± 5 (n = 10)*,#
HbA1c [%]	5.0 ± 0.1 (n = 16)	12.9 ± 0.3 (n = 15)*	8.6 ± 0.5 (n = 10)*,#	7.9 ± 0.4 (n = 10)*,#
Insulin [pg/ml], ELISA from serum w/o EDTA/ aprotinin	514 ± 57 (n = 14)	618 ± 128 (n = 14)	623 ± 79 (n = 9)	590 ± 94 (n = 9)
Insulin [pg/ml], RIA from plasma with EDTA/ aprotinin	343 ± 3 (n = 10)	590 ± 9 (n = 14)*	691 ± 16 (n = 8)*,#	853 ± 19 (n = 8)*,#,§
HOMA-IR index[b]	2.5 ± 0.3 (n = 10)	17.1 ± 2.8 (n = 13)*	10.8 ± 3.7 (n = 8)*	8.0 ± 1.9 (n = 8)*,#
HOMA-beta index [%][b]	62 ± 6 (n = 10)	15 ± 3 (n = 13)*	47 ± 15 (n = 8)#	90 ± 20 (n = 8)#
Glucagon [pg/ml], RIA from plasma with EDTA/ aprotinin	89 ± 5 (n = 10)	120 ± 7 (n = 10)*	103 ± 3 (n = 10)*	99 ± 6 (n = 8)#
Cholesterol [mg/dl], ELISA	91 ± 4 (n = 10)	246 ± 19 (n = 10)*	272 ± 19 (n = 10)*	269 ± 17 (n = 10)*
HDL [mg/dl], ELISA	31 ± 1 (n = 10)	75 ± 4 (n = 10)*	81 ± 3 (n = 10)*	80 ± 5 (n = 10)*
LDL [mg/dl], ELISA	44 ± 3 (n = 10)	60 ± 9 (n = 10)	63 ± 8 (n = 10)*	59 ± 11 (n = 10)
Triglycerides [mg/dl]	81 ± 7 (n = 10)	565 ± 69 (n = 10)*	677 ± 96 (n = 10)*	664 ± 63 (n = 10)*
Serum leptin [ng/ml], ELISA[c]	2.1 ± 0.6 (n = 5)	5.2 ± 0.5 (n = 5)*	8.9 ± 1.0 (n = 4)*,#	10.1 ± 1.7 (n = 4)*,#
Serum adiponectin [ng/ml], ELISA[c]	5.5 ± 0.5 (n = 5)	6.8 ± 0.5 (n = 5)	5.8 ± 0.5 (n = 4)	6.4 ± 0.5 (n = 5)
Serum methylglyoxal [μM], HPLC	0.23 ± 0.01 (n = 10)	0.34 ± 0.04 (n = 9)*	0.26 ± 0.02 (n = 10)#	0.25 ± 0.02 (n = 9)#
Serum CRP [μg/ml], ELISA	742 ± 44 (n = 12)	1057 ± 159 (n = 11)$^{p = 0.060 \text{ vs. Ctr}}$	673 ± 55 (n = 8)$^{p = 0.063 \text{ vs. ZDF}}$	653 ± 84 (n = 9)#

* $p < 0.05$ vs. control.
\# $p < 0.05$ vs. ZDF.
§ $p < 0.05$ vs. low dose SGLT2i treated.
[a] Non-fasting blood glucose was determined before SGLT2i treatment; fasting blood glucose as well as HbA1c levels were measured after SGLT2i treatment.
[b] HOMA-IR = [Glucose] * [Insulin] / 22.5 (fasting glucose in mmol/l; fasting insulin in mU/L); HOMA-beta = 20 * [Insulin] / ([Glucose] - 3.5) % (fasting glucose in mmol/l; fasting insulin in mU/L).
[c] Each samples pooled from 2 animals of the same group. The data are the means ± SEM of the indicated number of animals/group.

at higher levels in ZDF rats and decreased by both SGLT2i doses (Fig. 4D). AGE-positive renal proteins were also quantified by dot blot analysis in renal tissue and were elevated by trend in ZDF rats and dose-dependent normalization by SGLT2i treatment (not shown).

3.4. Protein expression

A surrogate parameter for the burden of oxidative stress is the level of 3-nitrotyrosine (3NT)- or 4-hydroxynonenal (HNE)-positive proteins. Immunohistochemical quantification of 3NT-positive proteins in aortic sections revealed an increase in ZDF rats, which was absent after SGLT2i treatment (Fig. 5A). Likewise, the expression levels of HNE-positive proteins in aortic and cardiac tissue were increased in untreated but not SGLT2i-treated ZDF rats (Fig. 5B-C). The expression of NADPH oxidase isoform Nox2 was increased in aorta of ZDF rats and reduced by SGLT2i treatment (Fig. 5D). The expression of NADPH oxidase isoform Nox1 was not changed in aorta of ZDF rats but showed a trend for decrease by 20–25% under SGLT2i treatment (not shown). In accordance with this observation, the general stress response and antioxidant enzyme, heme oxygenase-1 (HO-1) was upregulated in ZDF rats without treatment and reduced by low dose SGLT2i treatment (Fig. 5D). Another stress response enzyme under the control of NRF2, glutathione peroxidase-1 (GPx-1) was also upregulated in kidney of ZDF rats and reduced by low dose SGLT2i treatment (Fig. 5E). The inflammatory protein monocyte chemoattractant protein-1 (MCP-1 or CCL-2) was up-regulated in untreated but not SGLT2i-treated ZDF rats (Fig. 5D). Immunohistochemical quantification of CD68- and COX2-positive cells in aortic sections revealed an increase in ZDF rats (CD68 signal mainly in the adventitia, COX2 signal mainly in smooth muscle cells), which was rather not modified by SGLT2i treatment (not shown). More detailed mechanistic studies in vitro were hampered by the fact that we observed no effect of empagliflozin at reasonable doses (< 1 mM) on isolated human neutrophils (not shown). The contribution of advanced glycation end products (AGE) to the glucotoxicity in ZDF rats was assessed by expression levels of their receptors (RAGE) at the protein level (Fig. 5D). Aortic RAGE protein expression was increased in the aorta of ZDF rats and normalized by treatment (even below the levels in lean control rats). In support of increased AGE/RAGE signaling in ZDF rats, serum levels of the AGE precursor methylglyoxal were significantly increased in the ZDF group and improved by SGLT2i treatment (Table 1).

3.5. mRNA expression and epigenetic regulation

We also determined a number of inflammation markers by RT-PCR-based measurement of mRNA levels. Interferon-γ (IFN-γ) and cyclooxygenase-2 (COX2) expression was up-regulated in aorta of ZDF rats and both were reduced by SGLT2i treatment (Fig. 6A-B). Likewise, expression of inducible NO synthase (NOS2) and P-selectin (SELP; indicative of endothelial white blood cell attraction and infiltration as well as platelet activation and adhesion) were increased in aorta of ZDF rats and reduced by SGLT2i treatment (Fig. 6C and D). In line with these findings, the mRNA expression of the intercellular adhesion molecule-1 (ICAM-1) was up-regulated in the aorta of ZDF rats by 25% and normalized by the high dose SGLT2i therapy (not shown).

We also tested specific histone marks in promoter regions of genes of interest. In order to test whether our newly established ChIP procedure is working fine, we quantified the activating (H3K4me3) and suppressing (H3K9me3) histone marks in an always active gene (GAPDH) and in a genomic region, which is devoid of protein-coding genes (gene desert). In renal tissue H3K4me3 was high and H3K9me3 was low for GAPDH, whereas the opposite results were obtained for gene desert (not shown). The activating epigenetic mark histone3 lysine4 trimethylation (H3K4me3) was measured in the promoter region of *eNOS* and was found to be decreased in all ZDF groups (Fig. 6E). These data together with unaltered *eNOS* expression in renal tissue as

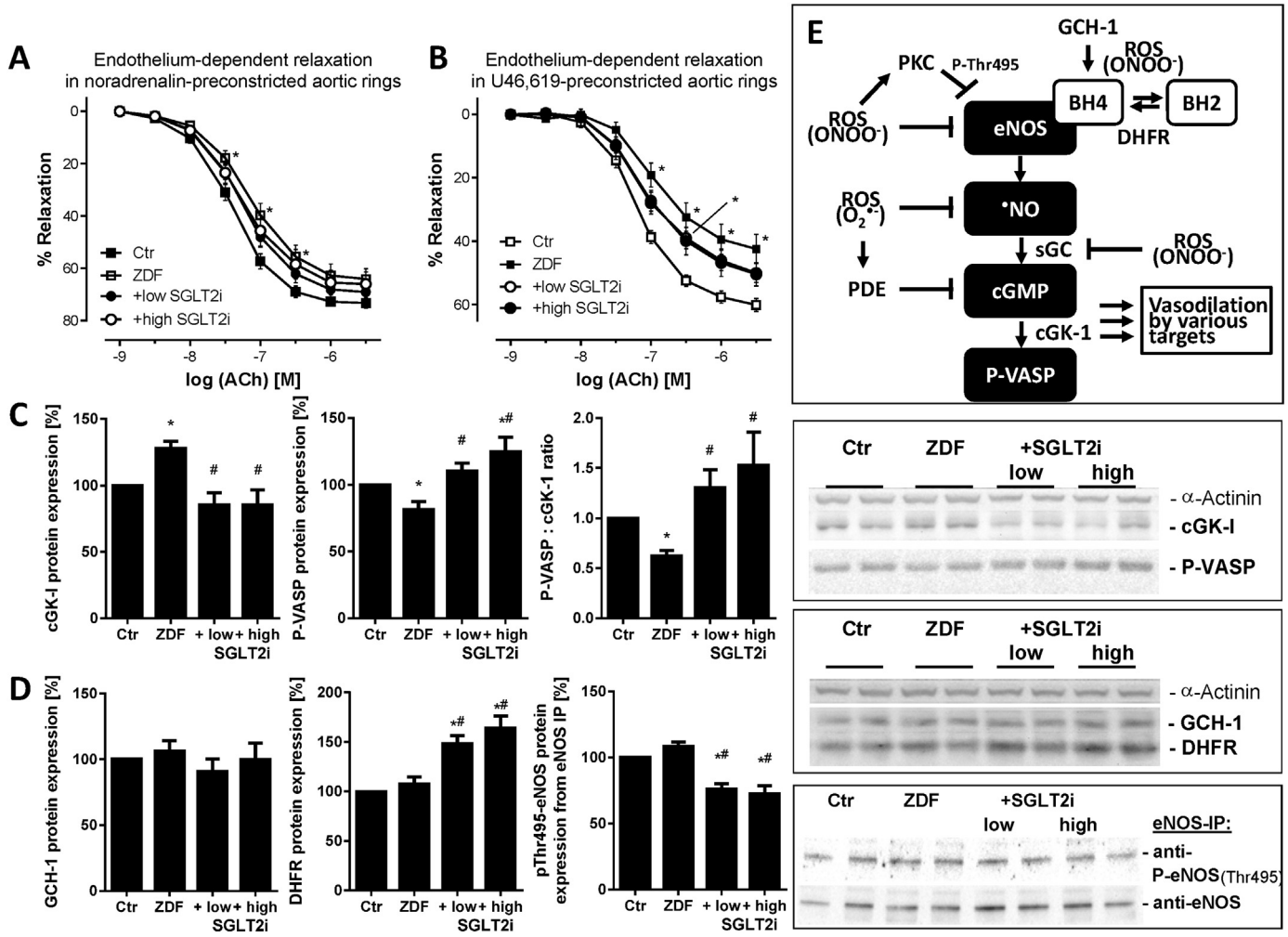

Fig. 2. Effects of SGLT2i treatment on vascular parameters in ZDF rats. Effects of SGLT2i treatment on endothelium-dependent relaxation by the vasodilators acetylcholine (ACh) in noradrenalin (**A**) or U46,619 (**B**) preconstricted aortic ring segments. Each single value for an animal corresponds to the means of 4 individual aortic rings from this animal. Protein expression of cGK-I, serine239 phosphorylated VASP and the resulting P-VASP/cGK-I ratio as a surrogate parameter for the integrity of vascular $^{\bullet}$NO/cGMP signaling was determined by Western blot analysis (**C**). Likewise, protein expression of the BH_4 regulating enzymes GCH-1 and DHFR as well as phosphorylation of eNOS at Thr495 (in immunoprecipitated eNOS) was determined as surrogate parameters for the coupling state of eNOS (**D**). Representative blots for all proteins are shown besides the densitometric quantification. (**E**) Scheme illustrating the $^{\bullet}$NO/cGMP signaling pathway leading to vasodilation with the major sites for its oxidative inactivation. BH4, tetrahydrobiopterin; cGK-1, cGMP-dependent protein kinase 1; DHFR, dihydrofolate reductase; GCH-1, GTP-cyclohydrolase-1; PDE, phosphodiesterase; PKC, protein kinase C; P-VASP, phosphorylated (Ser239) vasodilator stimulated phosphoprotein; ROS, reactive oxygen species. sGC, soluble guanylyl cyclase. Data are the means ± SEM from 9 to 12 animals/group (**A,B**) or from at least 4 independent experiments with pooled tissues from at least 8 animals/group (**C,D**). *, $p < 0.05$ vs. control and $^{\#}$, $p < 0.05$ vs. ZDF group. For the vascular function data the significance levels were determined by two-way-ANOVA for each ACh concentration.

measured by RT-PCR (not shown) underline that the partial rescue of endothelial function by empagliflozin is not due to upregulated eNOS expression but likely operates via improved $^{\bullet}$NO/cGMP signaling and by prevention of oxidative damage in this cascade. In contrast, empagliflozin groups displayed less H3K4me3 in the promoter regions of the inflammatory genes *IFN-γ* and *NOS2* (Fig. 6F and G). For *RAGE* at least a trend of decreased H3K4me3 in the promoter region of the gene was observed under empagliflozin therapy (Fig. 6H). Noteworthy, renal mRNA levels of *NOS2* showed a similar pattern as in aorta (not shown).

3.6. Hyperglycemia correlates with the primary pathologies in T2DM

The importance of glycemic control to prevent glucotoxicity as the primary pathology of T2DM is supported by the inverse correlation between fasting blood glucose levels or HbA1c values and endothelial function of aortic ring segments (Fig. 7A), and by the positive correlations between fasting blood glucose levels or HbA1c values leukocyte-dependent oxidative burst (as a read-out of the activation state of circulating phagocytes) and the inflammation marker CRP in serum (Fig. 7B-C), highlighting the therapeutic need for multi-targeted pharmacological approaches to prevent glucotoxicity at all levels. The activity of the cardioprotective protein ALDH-2 showed at least a stable trend for the inverse correlation with HbA1c values (Fig. 7D). In general, the correlations between HbA1c values and the measured parameters showed better statistical significance than those with blood glucose levels.

3.7. Evidence for pleiotropic effects of empagliflozin in cultured endothelial cells

The protective effects of empagliflozin (EMPA), the DPP-4 inhibitor sitagliptin (SITA) and the RAGE inhibitor FPS-ZM1 were compared head to head in cultured hyperglycemic human endothelial cells (HUVECs) by qualitative assessment of living cells (Fig. 8A and C). The density of the cells was decreased and their shape was changed to an elongated, activated (and in some cases apoptotic) state in the hyperglycemic groups from day 0 to day 6. In addition, many non-adherent, dead cells were observed in the high glucose wells ("white"

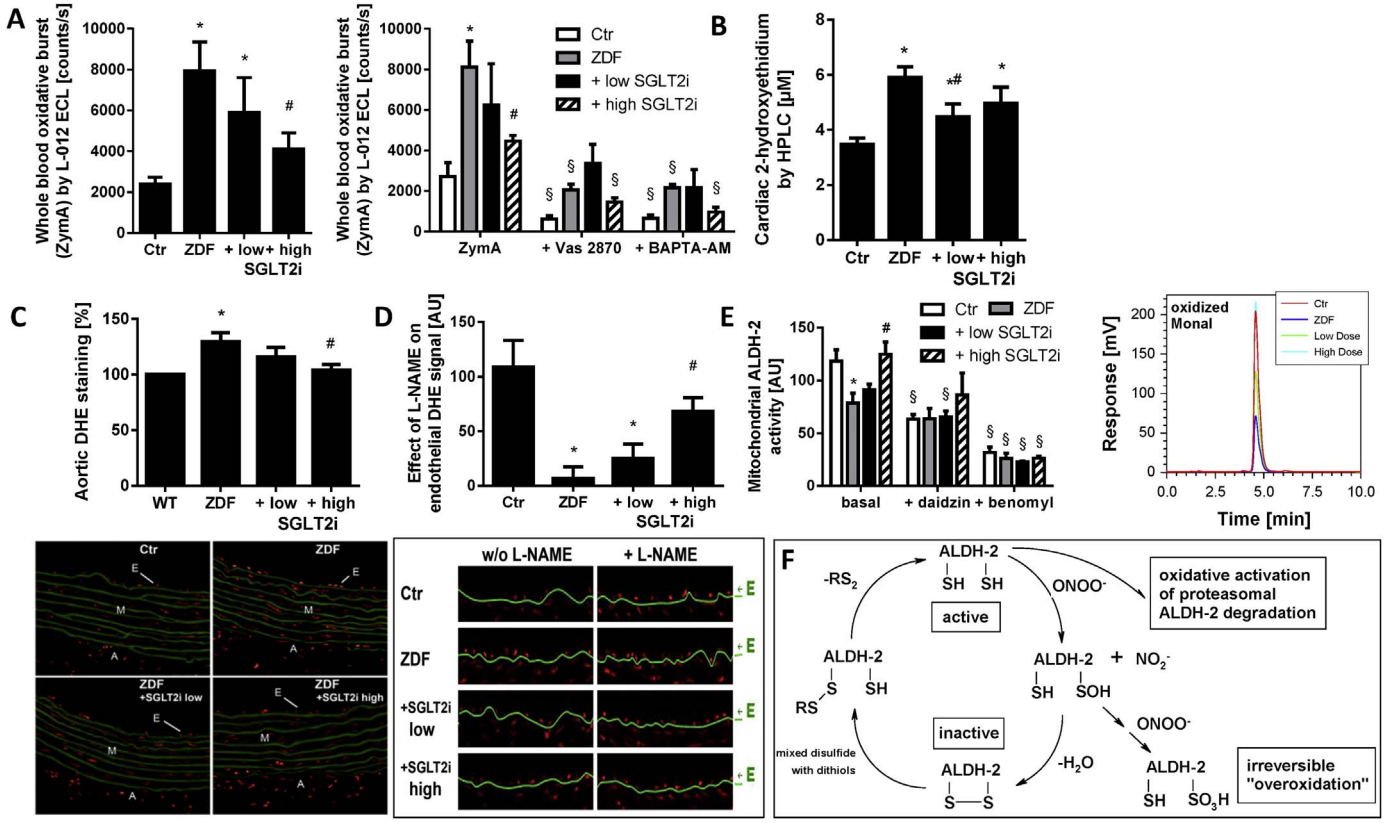

Fig. 3. Effects of SGLT2i treatment on oxidative stress parameters in ZDF rats. Leukocyte-derived ROS (oxidative burst) in whole blood at 30 min upon zymosan A stimulation along with the effects of the NADPH oxidase isoform 2 (Nox2) inhibitor VAS2870 and the intracellular calcium chelator BAPTA-AM (**A**). Quantification of cardiac NADPH oxidase activity in membrane preparations by dihydroethidium (50 µM)-derived fluorescent and superoxide-specific product 2-hydroxyethdium in the presence of NADPH (200 µM) by HPLC analysis (**B**). Dihydroethidium (DHE, 1 µM)-fluorescence microtopography was used to assess the effects of SGLT2i treatment on whole vascular wall (**C**) and endothelial (**D**) ROS production with and without incubation with the eNOS inhibitor L-NAME (0.5 mM). Representative microscope images are shown along with the densitometric quantification. Red fluorescence indicates ROS formation whereas green fluorescence represents basal laminae autofluorescence. Redox-sensitive, cardiac mitochondrial aldehyde dehydrogenase (ALDH-2) activity in ZDF rats was determined in isolated heart mitochondria by conversion of Monal 62 to its fluorescent naphthoic acid product (**E**). Daidzin (50 µM) is a specific ALDH-2 inhibitor, whereas benomyl (10 µM) is an unspecific ALDH inhibitor. Representative chromatograms are shown along with the quantification. (**F**) Scheme illustrating the oxidative inactivation of the mitochondrial aldehyde dehydrogenase (ALDH-2) via disulfide bridge formation (reversible inhibition) and sulfonic acid product (irreversible inhibition). Data are the means ± SEM from 9 w/o inhibitor (**A**), 3 with inhibitor (**A**), 6–8 (**B**), 5–6 (**C,D**) or 4 (**E**) animals/group. *, $p < 0.05$ vs. control and $^{\#}$, $p < 0.05$ vs. ZDF group and §, $p < 0.05$ vs. corresponding group w/o inhibitor.

cells). Especially the higher (supra-pharmacological) concentrations of empagliflozin and the dipeptidyl peptidase-4 sitagliptin conferred obvious protection against glucotoxicity and normalized the cell density and shape almost completely, indicating potent pleiotropic effects on hyperglycemic endothelial cells (a glucose decrease in the medium can be excluded). The RAGE inhibitor FPS-ZM1 showed an intermediate effect at least demonstrating the therapeutic potential of interruption of the AGE/RAGE signaling pathway.

As a read-out of functional eNOS, the formation of nitrite upon stimulation of the cells with acetylcholine was determined. In accordance with the data on cell shape and density, the nitrite formation by HUVECs was sharply decreased under hyperglycemic conditions and restored by all drugs in a concentration-dependent fashion (Fig. 8B). Although only minor differences between the drugs were observed, EMPA was slightly more beneficial than SITA and the RAGE inhibitor FPS-ZM1. We would like to stress that the eNOS-dependent nitrite formation was decreased by 85% in hyperglycemic HUVECs, whereas the cell number was only diminished by 71% indicating that the functional loss was more pronounced than expected by the loss of cells. Likewise, the recovery of nitrite formation under drug treatment was more pronounced than the gain in cell number implying that the drugs not only prevent cell death but also improve eNOS function.

4. Discussion

Our study demonstrates that chronic treatment of ZDF rats with the SGLT2i empagliflozin prevents the development of oxidative stress, AGE/RAGE signaling and inflammation, and also partially improved endothelial function in a well characterized animal model of type 2 diabetes mellitus. These beneficial effects are likely due to glucose lowering effects but also improved glucose utilization by restored insulin sensitivity and signaling, all of which prevent down-stream glucotoxicity such as AGE formation, AGE/RAGE signaling, metabolic dysfunction, oxidative stress, inflammation and impairment of vascular function (reflected by the correlations shown in Fig. 7). Improvement of the redox state should contribute to reduced β-cell apoptosis and improved insulin production.

Importantly, the efficacy of some of the current anti-diabetic treatments vanishes over time, leading to a progression of the disease [20]. This phenomenon is mostly explained by progression of β-cell apoptosis and dysfunction in the setting of diabetes, which is efficiently prevented by empagliflozin and other SGLT2i therapy [27,42,43]. SGLT2i therapy preserves β-cell integrity and functional capacity as shown by our immunohistological and -histochemical analysis. Our data also show that α-cells of the pancreatic islets and their glucagon content are preserved suggesting that empagliflozin treatment preserves the two major mechanisms involved in the glucose homeostasis. Young, prediabetic, ZDF rats (< 14 weeks) have significantly increased plasma insulin levels compared to their wild-type littermates to compensate for insulin resistance (hyperinsulinemia), whereas in older ZDF rats, plasma insulin levels continuously decline in parallel with progressing β-cell dysfunction due to oxidative and glucotoxic damage as

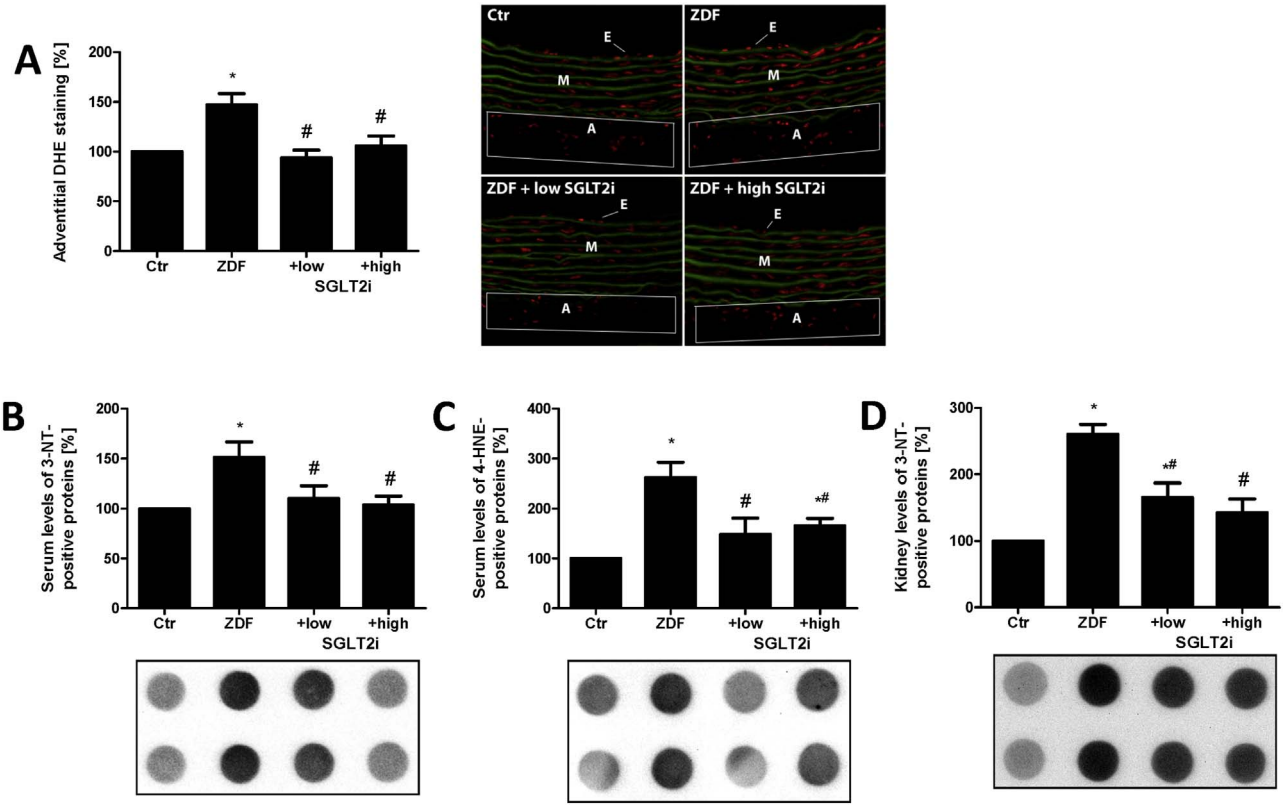

Fig. 4. Effects of SGLT2i treatment on adventitial ROS formation and serum / kidney protein modifications involved in oxidative stress pathways in ZDF rats. Dihydroethidium (DHE, 1 μM)-fluorescence microtopography was used to assess the effects of SGLT2i treatment on adventitial ROS production (**A**). 3-nitrotyrosine (3-NT)-positive (**B**) and 4-hydroxynonenal (HNE)-positive (**C**) proteins were measured by dot blot analysis in serum samples. Representative blots are shown below the densitometric quantification. 3-nitrotyrosine (3-NT)-positive proteins (**D**) was measured by dot blot analysis in renal tissue. Representative blots are shown below the densitometric quantification. The data are the means ± SEM from 6 to 8 (**A**) or 6–8 (**B-D**) animals/group. *, $p < 0.05$ vs. control and #, $p < 0.05$ vs. ZDF group.

well as exhaustion of insulin content [44,45]. However, insulin-sensitivity is not fully restored as shown by the only partially normalized blood glucose values (fasting and non-fasting) and HbA1c values as well as the obvious hyperinsulinemia in the plasma of all ZDF groups. The increase in insulin plasma levels in ZDF rats with different SGLT2i drugs is well documented [25,46–49]. Of importance is that empagliflozin was shown to lower blood glucose levels (thereby sparing insulin) in a preclinical model of streptozotocin-induced type 1 diabetes [50] and also in human studies [51,52].

SGLT2i treatment appears to be highly efficient in preventing glucotoxicity, i.e. increased methylglyoxal levels, formation of AGE and the induction of RAGE-dependent signaling. Importantly, methylglyoxal has recently been demonstrated to play an essential role in the development and progression of diabetic neuropathy in diabetic mice and patients, and therefore represents a target of special interest for pharmacological modulation [53]. Increased AGE/RAGE signaling was reported for diabetic rats [54], which contributes to oxidative stress and vascular complications [55] via activation of NADPH oxidases [12] and impairment of $^{\bullet}$NO/cGMP signaling [55]. Our data support impaired $^{\bullet}$NO/cGMP signaling (as suggested by reduced P(Ser239)-VASP levels, the substrate of cGMP-dependent protein kinase (cGK-1)) with vascular dysfunction (for detailed mechanism see Fig. 2E), which is best explained by direct oxidative inactivation of the constituents of this pathway (e.g. thiol oxidation in sGC, oxidative break-down of $^{\bullet}$NO, and oxidative depletion of BH4) [56,57] but also adverse phosphorylation of eNOS at Thr495 by protein kinase C [40,41]. Our ChIP data on histone modification at the eNOS promoter show that the activating H3K4me3 mark is decreased throughout all ZDF groups and not restored by SGLT2i treatment supporting that improved $^{\bullet}$NO/cGMP signaling by empagliflozin is not based on upregulation of eNOS gene but potentially on prevention of oxidative damage of the $^{\bullet}$NO/cGMP signaling pathway. Likewise, RAGE-antagonism improved late-stage diabetic complications such as hind limb ischemia in T1DM mice [58], nephropathy in ZDF rats [59–61] and microvascular damage in T1DM rats [62].

According to previous data AGE/RAGE signaling triggers low-grade inflammation [16] as supported by the protein and mRNA expression data and oxidative stress measurements of this study. All of these adverse effects were normalized by SGLT2i treatment in accordance with the previously reported anti-inflammatory effects of empagliflozin in a model of atherosclerosis [63]. It should be noted that also other recent anti-diabetic drugs provide efficient glycemic control in diabetic conditions as reported for linagliptin and sitagliptin and other dipeptidyl peptidase-4 inhibitors, in ZDF and obese rats [64–66].

In the present study, the interplay between AGE/RAGE signaling, oxidative stress and inflammation is reflected by increased oxidative stress markers in various tissues and whole blood. We observed increased ROS formation in aorta, heart, kidney, serum and whole blood. In addition, we show that empagliflozin, sitagliptin and the RAGE inhibitor FPS-ZM1 improved viability and $^{\bullet}$NO formation in HUVECs under hyperglycemic conditions. The partial protection provided by the RAGE inhibitor underlines the significant contribution of AGE/RAGE signaling to the underlying pathophysiology of hyperglycemia and glucotoxicity, which is also reflected by the above discussed therapeutic efficacy of RAGE antagonists in diabetic animals.

Interestingly, ROS formation in the adventitia, as an example for adipose tissue, was increased, which could be associated with dysregulated adipokine synthesis. Here, we observed increased leptin levels in ZDF rats, which were not corrected by empagliflozin therapy. However, the meaning of this result is unclear in leptin receptor deficient rats (ZDF). In the present study, adiponectin levels were not changed significantly in any group as reported previously by others for

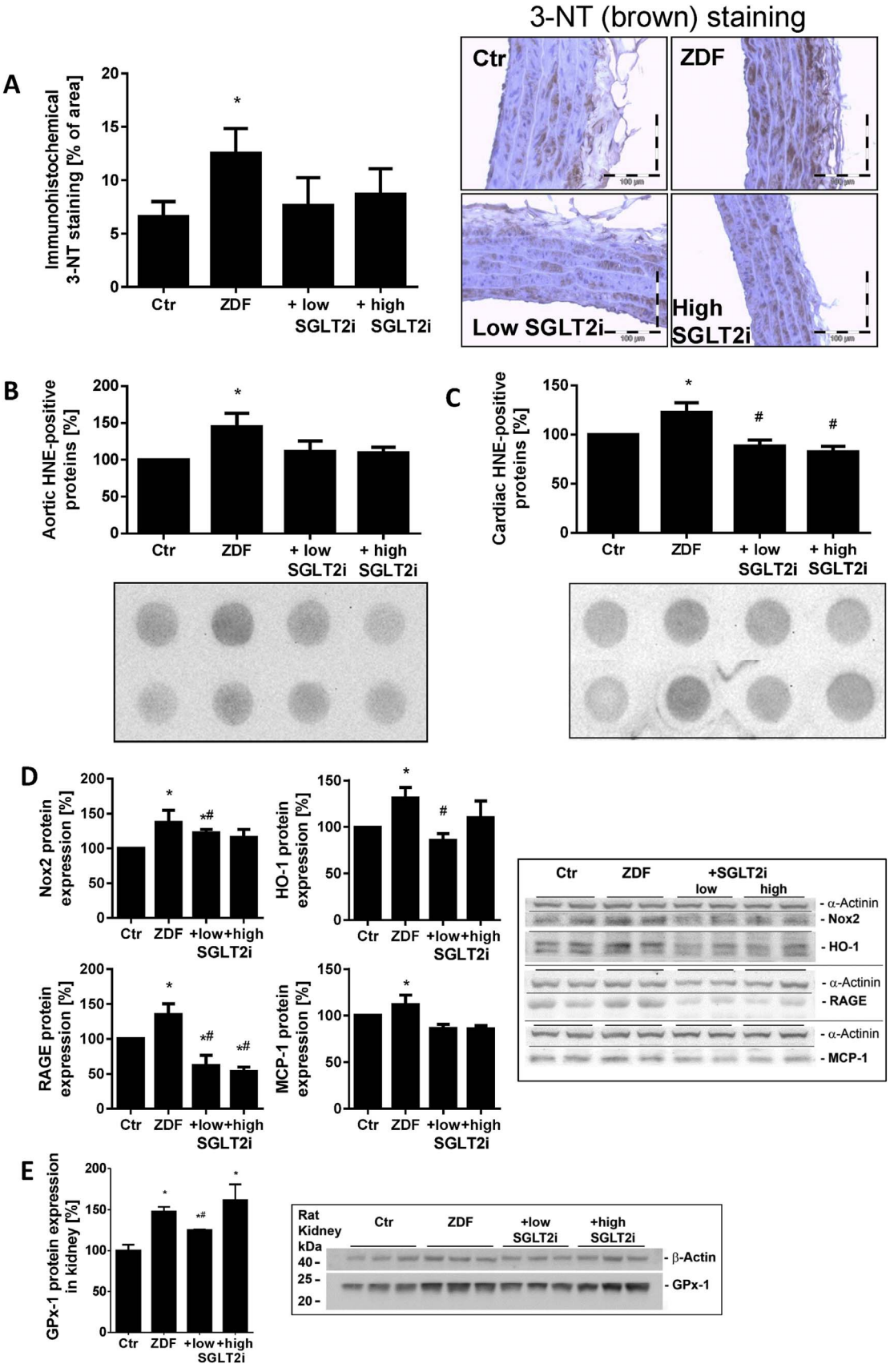

(caption on next page)

Fig. 5. Effects of SGLT2i treatment on aortic and cardiac protein expression / modification involved in oxidative stress and inflammatory pathways in ZDF rats. Levels of 3-nitrotyrosine (3-NT)-positive proteins was determined by immunohistochemical quantification in aortic sections (**A**). Representative pictures are shown along with the densitometric quantification. 4-hydroxynonenal (HNE)-positive proteins were measured by dot blot analysis in aortic (**B**) and cardiac (**C**) tissue. Representative blots are shown below the densitometric quantification. Aortic protein expression of the NADPH oxidase isoform Nox2, the antioxidant stress-response-enzyme heme oxygenase-1 (HO-1), the receptor for advanced glycation end products (RAGE) and the inflammatory signaling protein monocyte-chemoattractant-protein-1 (MCP-1 or CCL-2) was assessed by Western blotting analysis and specific antibodies (**D**). Renal protein expression of the antioxidant stress-response-enzyme glutathione peroxidase-1 (GPx-1) was assessed by Western blotting analysis and specific antibodies (**E**). Representative blots for all proteins are shown along with the densitometric quantification. The data are the means ± SEM from 7 (**A**) or 4–6 (**B,C,D,E**) animals/group. *, $p < 0.05$ vs. control and #, $p < 0.05$ vs. ZDF group.

old ZDF rats [67], for empagliflozin in obese rats [26] and for dapagliflozin therapy in T2DM patients [68]. Whether these obvious paradoxical observations contribute to the increase of triglycerides and cholesterol under empagliflozin therapy remains to be established. Triglycerides are more often reported to be diminished in response to empagliflozin therapy in humans [22].

Related to the here reported direct oxidative stress parameters, the redox regulated enzyme, mitochondrial aldehyde dehydrogenase (ALDH-2), is not only important as a nitroglycerin bioactivating enzyme [69,70] but also degrades toxic aldehydes such as acetaldehyde, malondialdehyde and 4-hydroxynonenal [71]. Recent studies show that ALDH-2 plays an important role in the reduction of myocardial damage during ischemia/reperfusion thereby reducing the infarct size [72] and confers cardio-protection in an experimental diabetes/myocardial infarction model [73]. ALDH-2 deficiency was associated with increased ROS formation in aging animals [74], alcohol-induced heart failure [75] and acetaldehyde overload as well as nitroglycerin challenges [76]. In the setting of nitroglycerin-induced nitrate tolerance oxidatively triggered proteasomal degradation of ALDH-2 protein was reported [77]. Therefore, the inactivation and/or down-regulation of ALDH-2 in the ZDF group strongly supports the cardio-toxic phenotype of hyperglycemia and the improved activity of this redox-sensitive enzyme with high dose SGLT2i treatment supports cardio-protective and antioxidant properties of this drug.

ZDF rats are used as a model of T2DM for more than 35 years. Here, we would like to discuss some major strengths and limitations of this animal model. ZDF rats display a severe phenotype of T2DM with all known features of this disease and strong parallels to the metabolic syndrome. This is an inbred animal model in which the genetic background is homogenous and exogenous factors are minimized (e.g. as encountered during surgery and drug administration to induce diabetes in other models). As a general note we would like to mention that despite the fact that the ZDF model has been used for a quite long time as a model of T2DM, there is still large variation in multiple parameters (e.g. insulin levels, CRP). These differences could be due to the pronounced time course underlying the T2DM features in ZDF rats and researchers using the rats at different time points as well as the quality of the assays used (here we show significant differences for measurement of plasma/serum insulin levels by using ELISA without protease inhibitors and RIA with protease inhibitors). For the purpose of illustration, large variations for the measurement of body weight, HbA1c values, serum insulin levels, HOMA-IR and HOMA-beta, as well as serum CRP levels were found in publications describing the ZDF phenotype. The major part of these variations may be ascribed to the different age of investigated ZDF rats (due to the above mentioned time course underlying the pathologies) but also the use of different ELISAs as well as different approaches for the complicated calculation and conversion of HOMA-IR, HOMA-beta and insulin values. Besides these inherent problems linked to the use of the ZDF model (as with most animal models), the high animal costs and increased mortality due to ketosis at advanced age and the absence of the leptin receptors could lead to compensatory increases in leptin levels and the loss of leptin effects in various adipokine signaling pathways (e.g. regulation of circulating cortisol). A summary of advantages and disadvantages of the ZDF model is provided in a detailed overview [78].

Interestingly, despite being a specific SGLT2 inhibitor and causing a dramatic increase in urine volume and glucose excretion in non-diabetic mice, previous studies showed that urine volume and glucose excretion in db/db mice were not changed by chronic empagliflozin treatment [49]. Ojima et al. found that HbA1c and fasting blood glucose

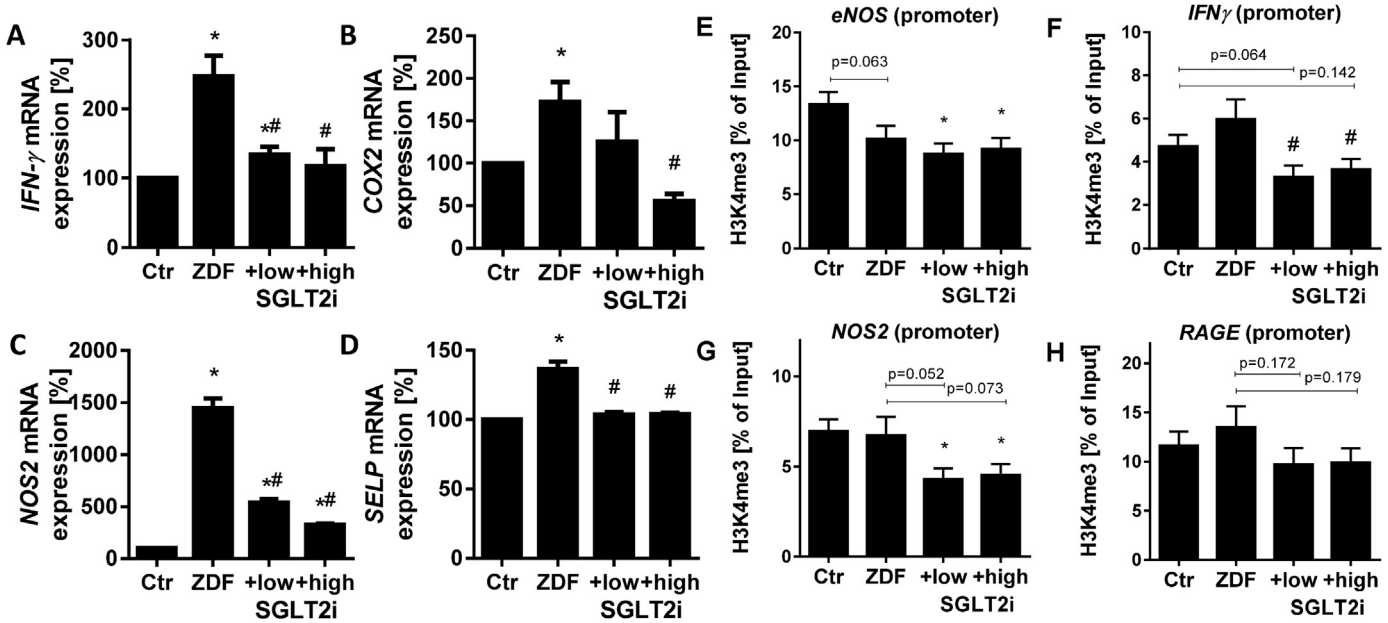

Fig. 6. Effects of SGLT2i treatment on aortic mRNA expression of pro-inflammatory genes epigenetic regulation in ZDF rats. mRNA expression of inflammatory genes *interferon-γ* (*IFN-γ*, **A**), *cyclooxygenase-2* (*COX2*, **B**), *inducible NO synthase* (*NOS2*, **C**) and a marker for vascular immune cell attraction as well as for platelet and endothelial activation *P-selectin* (*SELP*, **D**) was assessed by quantitative RT-PCR. The data are expressed as % of control and are the means ± SEM from at least 3 (**A-D**) animals/group. The activating epigenetic mark histone3 lysine4 trimethylation (H3K4me3) was measured in the promoter regions of *eNOS* (**E**), *IFN-γ* (**F**), *NOS2* (**G**) and *RAGE* (**H**) by ChIP. The data are expressed as % of input and are the means ± SEM from 9 to 14 animals/group (**E-H**). *, $p < 0.05$ vs. control and #, $p < 0.05$ vs. ZDF group.

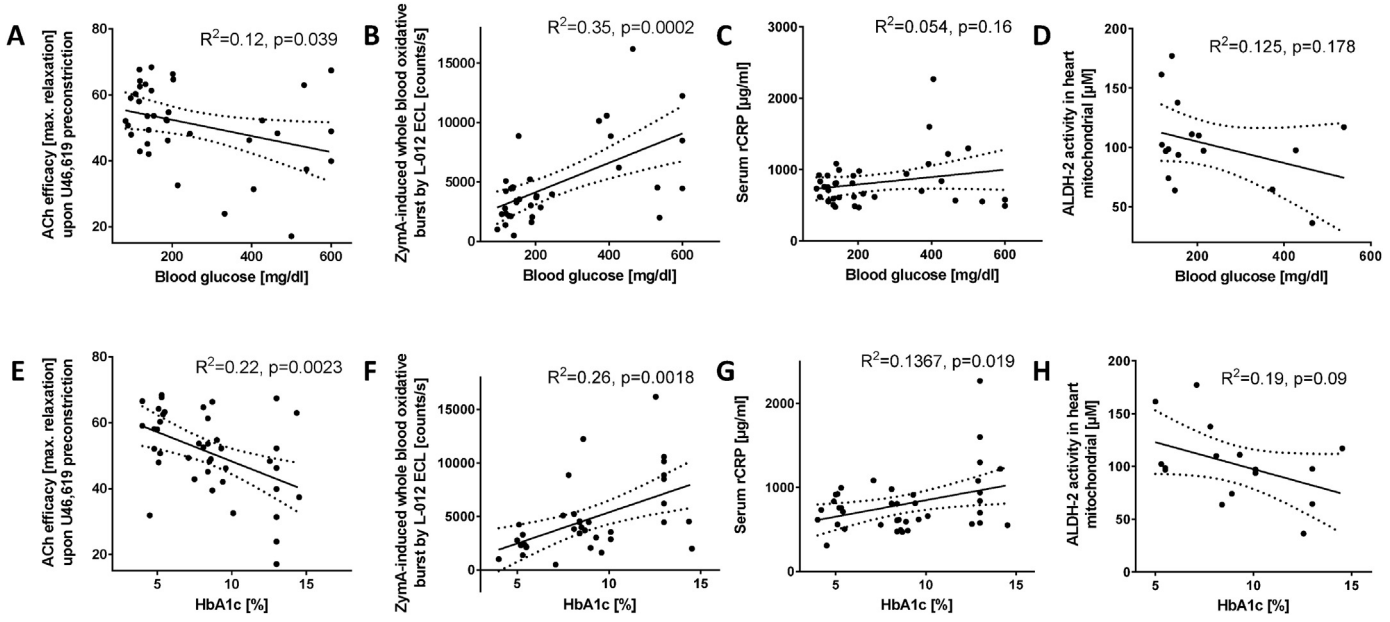

Fig. 7. Linear regression analysis for correlations between fasting blood glucose (**A-D**) or HbA1c (**E-H**) and endothelial function (ACh efficacy, **A and E**), zymosan A-induced whole blood oxidative burst **(B, F)**, serum CRP levels **(C, G)** or ALDH-2 activity **(D, H)**. The total number of data sets (animals) for linear regression analysis was 37 (**A**), 35 (**B**), 38 (**C**), 16 (D), 41 (**E**), 35 (**F**), 40 (**G**) and 16 (**H**). p-values and correlation coefficients (R^2) are provided in the graphs.

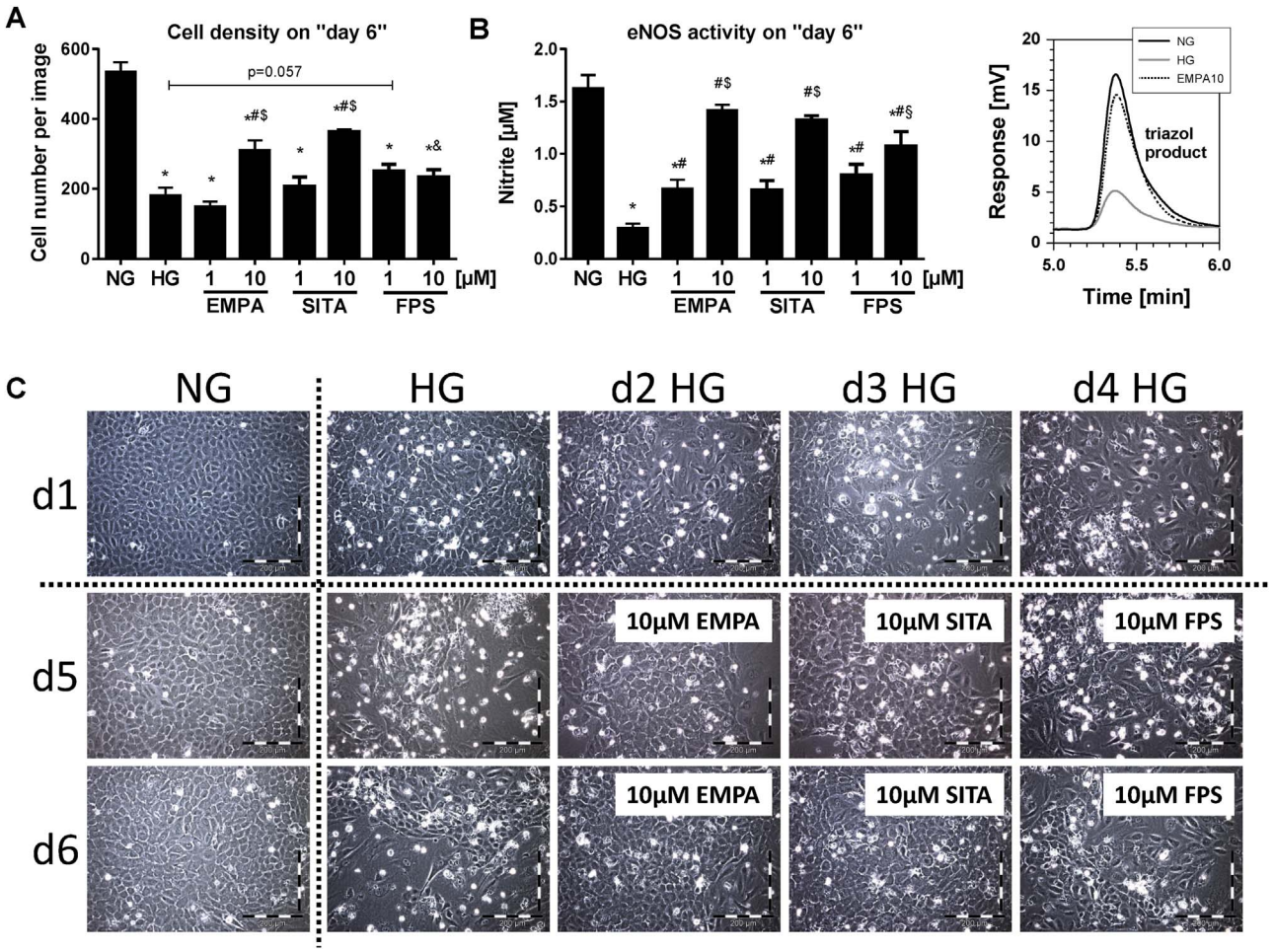

Fig. 8. Experiments in cultured human endothelial cells reveal pleiotropic effects of empagliflozin. The protective effects of empagliflozin (EMPA), the DPP-4 inhibitor sitagliptin (SITA) and the RAGE inhibitor FPS-ZM1 were tested in cultured hyperglycemic human endothelial cells (HUVECs) by qualitative and quantitative assessment of living cells (density and shape) (**A, C**). Representative pictures of cells are shown. Nitrite formation in response to acetylcholine (1 µM) in the supernatant was determined by acidic conversion of 2,3-diaminonaphthalene to the triazol product and HPLC-based quantification using fluorescent detection (**B**). Representative chromatograms are shown besides the quantitative data. The data are the means ± SEM from at least 5 independent experiments. *, $p < 0.05$ vs. NG; #, $p < 0.05$ vs. HG; $, $p < 0.05$ vs. same 1 µM group; §, $p < 0.05$ vs. EMPA10; &, $p < 0.05$ vs. SITA10.

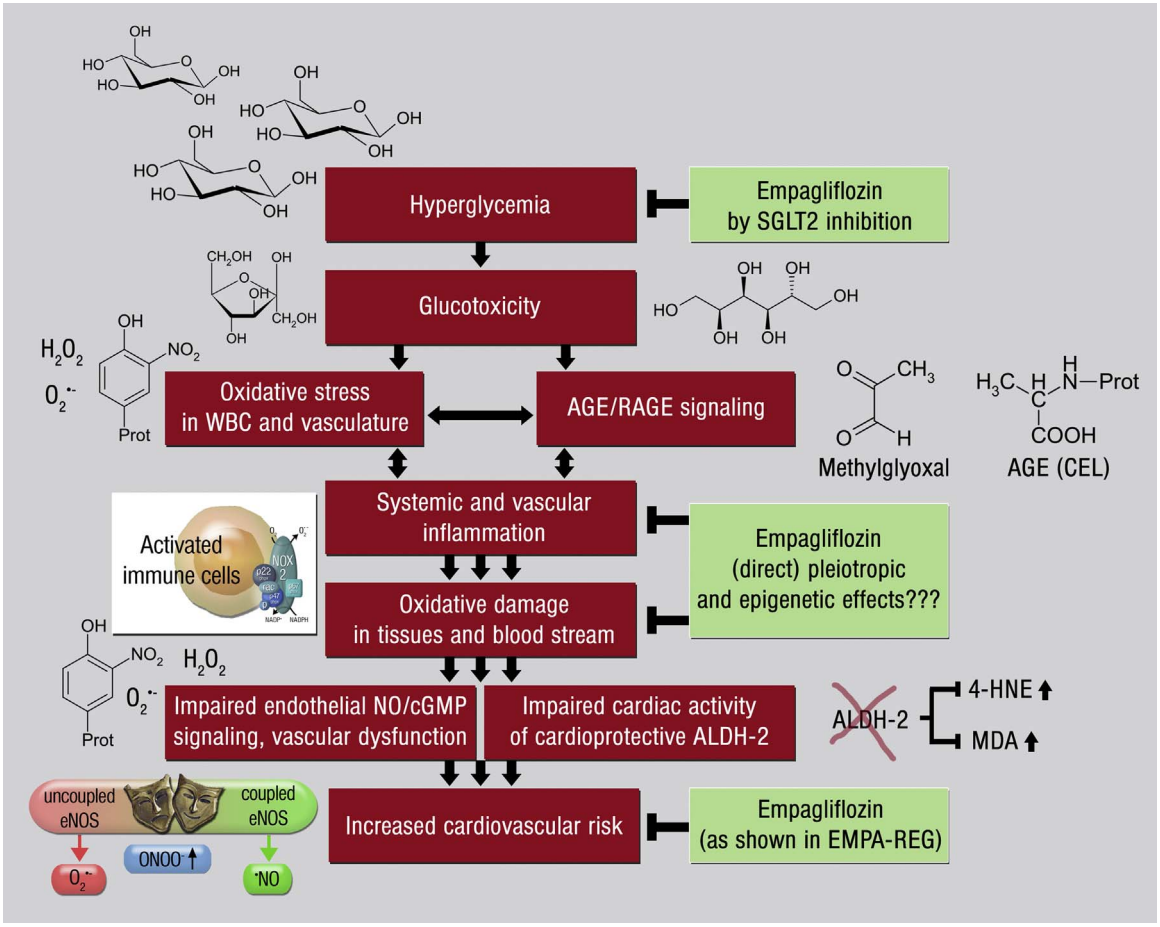

Fig. 9. Hypothetical scheme on empagliflozin-conferred protection in T2DM. The normalization of the glycemic condition and prevention of glucotoxicity are the major beneficial properties of empagliflozin and other SGLT2i but (direct) epigenetic and pleiotropic effects may also contribute. The secondary pathologies oxidative stress, AGE/RAGE signaling, inflammation with subsequent vascular dysfunction and increased cardiovascular risk are accordingly improved by the primary action of empagliflozin (the latter shown by the EMPA-REG trial).

values were significantly decreased by empagliflozin but glucosuria was not diminished in STZ rats [79]. In humans at least the urine excretion volume is not significantly changed by empagliflozin [80]. These data question urine volume and glucose excretion as reliable parameters in animal models of T2DM. A potential limitation of our in vitro experiments in cultured HUVECs is the fact that the employed empagliflozin concentrations were supra-pharmacological (1 and 10 μM) as compared to the circulating levels expected in our empagliflozin treated rats (approximately 100–250 nM). However, it should be noted that concentrations of 1–100 μM of empagliflozin and other SGLT2i are frequently used in cell culture [81,82]. Another limitation of the cell culture studies in HUVECs is the lack of knowledge of the presence and function of SGLT2 in endothelial cells. Accordingly, we consider the effects of empagliflozin observed in our cell culture to be of "pleiotropic" nature, although final proof on the exact mechanism of empagliflozin and sitagliptin mediated improvements (e.g. via better glucose utilization and respective anti-hyperglycemic effects or via direct modulation of the down-stream glucotoxicity by reduction of oxidative stress, inflammation and AGE/RAGE signaling) requires further investigation. The protective effects of the RAGE inhibitor FPS-ZM1 demonstrate the importance of the AGE/RAGE axis for hyperglycemia-induced complications.

Another caveat and limitation of SGLT2i treatment could be that the observed hypercholesterolemia in ZDF rats was not improved by empagliflozin providing a feasible explanation for the moderate improvement of some of the parameters (including endothelial function) and suggesting a therapeutic approach for T2DM (metabolic syndrome) that combines SGLT2i and lipid-lowering drugs. Importantly, we here provide evidence for decreased epigenetic activation of *NOS2* and *IFNγ* (for *RAGE* by trend) due to decreased H3K4me3 in the promoter regions of the genes in kidneys of SGLT2i treated ZDF rats. It has been shown previously that global differences in H3K4 trimethylation are associated with overweight and type 2 diabetes [83]. In addition, studies in diabetic patients showed increased promoter H3K9me2 in genes that are associated with autoimmune and inflammation-related pathways, such as transforming growth factor-beta (TGFβ), nuclear factor-κB, p38 mitogen-activated protein kinase, toll-like receptor, and interleukin-6 [84]. Our present data cannot clarify whether these epigenetic effects are a consequence of glucose lowering and would be shared by most other antidiabetic drugs, conferring glycemic control, or represent a specific (direct, pleiotropic) property of empagliflozin. A head-to-head comparison of different antidiabetic drugs (e.g. empagliflozin, sitagliptin and FPS-ZM1) in vivo are necessary to answer this question.

In summary, the results of our study confirm previous findings on correlations between vascular oxidative stress, AGE/RAGE signaling, low-grade inflammation and vascular dysfunction in diabetic animals or patients and highlight the importance of glycemic control to prevent glucotoxicity as the primary pathology of T2DM (Fig. 9). Epigenetic but also pleiotropic effects of empagliflozin may contribute to this beneficial pharmacological profile. The importance of our preclinical data is underlined by a recent large clinical trial where the major finding was that empagliflozin reduces the cardiovascular and overall mortality in T2DM patients at high cardiovascular risk (EMPA-REG) [2,22], which makes inhibition of SGLT2 an attractive anti-diabetic therapy and warrants further exploration in combination therapeutic approaches.

Financial support

The present work was supported by a vascular biology research grant from Boehringer Ingelheim Pharma GmbH & Co. KG, Ingelheim, Germany (A.D. and T.M.), by the Federal Ministry of Education and Research (grant 01EO1503 to S.S. and P.W.) and by the Center of Translational Vascular Biology (CTVB) of the University Medical Center Mainz, Germany. A.H. holds a stipend from the International PhD Program on the "Dynamics of Gene Regulation, Epigenetics and DNA Damage Response" from the Institute of Molecular Biology gGmbH, (Mainz, Germany) funded by the Boehringer Ingelheim Foundation.

Conflicts of interest

T.M. and A.D. received research grants from Boehringer Ingelheim Pharma GmbH & Co. KG. E.M. is an employee of Boehringer Ingelheim Pharma GmbH & Co. KG. The remaining authors declare that they have no competing interests in connection with this manuscript.

Acknowledgments

We are indebted to Angelica Karpi, Jörg Schreiner, Jessica Rudolph, Nicole Glas and Bettina Mros for expert technical assistance (all from the University Medical Center Mainz, 55131 Mainz, Germany). We thank Margot Neuser for graphical assistance. This paper contains results that are part of the doctoral thesis of Philipp Welschof (serum methylglyoxal, aortic RAGE protein expression, and laboratory parameters) and of the doctoral thesis of Alina Hanf (ChIP data, HUVEC data, protein and functional data).

References

[1] D.M. Nathan, P.A. Cleary, J.Y. Backlund, S.M. Genuth, J.M. Lachin, T.J. Orchard, P. Raskin, B. Zinman, Intensive diabetes treatment and cardiovascular disease in patients with type 1 diabetes, N. Engl. J. Med. 353 (2005) 2643–2653.

[2] B. Zinman, C. Wanner, J.M. Lachin, D. Fitchett, E. Bluhmki, S. Hantel, M. Mattheus, T. Devins, O.E. Johansen, H.J. Woerle, U.C. Broedl, S.E. Inzucchi, E.-R. O. investigators, empagliflozin, cardiovascular outcomes, and mortality in type 2 diabetes, N. Engl. J. Med. 373 (2015) 2117–2128.

[3] D. Jay, H. Hitomi, K.K. Griendling, Oxidative stress and diabetic cardiovascular complications, Free Radic. Biol. Med. 40 (2006) 183–192.

[4] U. Hink, H. Li, H. Mollnau, M. Oelze, E. Matheis, M. Hartmann, M. Skatchkov, F. Thaiss, R.A. Stahl, A. Warnholtz, T. Meinertz, K. Griendling, D.G. Harrison, U. Forstermann, T. Munzel, Mechanisms underlying endothelial dysfunction in diabetes mellitus, Circ. Res. 88 (2001) E14–E22.

[5] M.H. Zou, C. Shi, R.A. Cohen, Oxidation of the zinc-thiolate complex and uncoupling of endothelial nitric oxide synthase by peroxynitrite, J. Clin. Investig. 109 (2002) 817–826.

[6] N.J. Alp, S. Mussa, J. Khoo, S. Cai, T. Guzik, A. Jefferson, N. Goh, K.A. Rockett, K.M. Channon, Tetrahydrobiopterin-dependent preservation of nitric oxide-mediated endothelial function in diabetes by targeted transgenic GTP-cyclohydrolase I overexpression, J. Clin. Investig. 112 (2003) 725–735.

[7] T. Heitzer, K. Krohn, S. Albers, T. Meinertz, Tetrahydrobiopterin improves endothelium-dependent vasodilation by increasing nitric oxide activity in patients with Type II diabetes mellitus, Diabetologia 43 (2000) 1435–1438.

[8] J. Cassuto, H. Dou, I. Czikora, A. Szabo, V.S. Patel, V. Kamath, E. Belin de Chantemele, A. Feher, M.J. Romero, Z. Bagi, Peroxynitrite disrupts endothelial caveolae leading to eNOS uncoupling and diminished flow-mediated dilation in coronary arterioles of diabetic patients, Diabetes 63 (2014) 1381–1393.

[9] J.M. Forbes, M.E. Cooper, V. Thallas, W.C. Burns, M.C. Thomas, G.C. Brammar, F. Lee, S.L. Grant, L.A. Burrell, G. Jerums, T.M. Osicka, Reduction of the accumulation of advanced glycation end products by ACE inhibition in experimental diabetic nephropathy, Diabetes 51 (2002) 3274–3282.

[10] Y. Yamamoto, S. Yamagishi, H. Yonekura, T. Doi, H. Tsuji, I. Kato, S. Takasawa, H. Okamoto, J. Abedin, N. Tanaka, S. Sakurai, H. Migita, H. Unoki, H. Wang, T. Zenda, P.S. Wu, Y. Segawa, T. Higashide, K. Kawasaki, H. Yamamoto, Roles of the age-RAGE system in vascular injury in diabetes, Ann. N. Y Acad. Sci. 902 (163–170) (2000) (discussion170-162).

[11] M.T. Coughlan, D.R. Thorburn, S.A. Penfold, A. Laskowski, B.E. Harcourt, K.C. Sourris, A.L. Tan, K. Fukami, V. Thallas-Bonke, P.P. Nawroth, M. Brownlee, A. Bierhaus, M.E. Cooper, J.M. Forbes, RAGE-induced cytosolic ROS promote mitochondrial superoxide generation in diabetes, J. Am. Soc. Nephrol. 20 (2009) 742–752.

[12] M.P. Wautier, O. Chappey, S. Corda, D.M. Stern, A.M. Schmidt, J.L. Wautier, Activation of NADPH oxidase by age links oxidant stress to altered gene expression via RAGE, Am. J. Physiol. Endocrinol. Metab. 280 (2001) E685–E694.

[13] T. Nishikawa, D. Edelstein, X.L. Du, S. Yamagishi, T. Matsumura, Y. Kaneda, M.A. Yorek, D. Beebe, P.J. Oates, H.P. Hammes, I. Giardino, M. Brownlee, Normalizing mitochondrial superoxide production blocks three pathways of hyperglycaemic damage, Nature 404 (2000) 787–790.

[14] E. Schulz, P. Wenzel, T. Munzel, A. Daiber, Mitochondrial redox signaling: interaction of mitochondrial reactive oxygen species with other sources of oxidative stress, Antioxid. Redox Signal 20 (2014) 308–324.

[15] S. Kroller-Schon, S. Steven, S. Kossmann, A. Scholz, S. Daub, M. Oelze, N. Xia, M. Hausding, Y. Mikhed, E. Zinssius, M. Mader, P. Stamm, N. Treiber, K. Scharffetter-Kochanek, H. Li, E. Schulz, P. Wenzel, T. Munzel, A. Daiber, Molecular mechanisms of the crosstalk between mitochondria and NADPH oxidase through reactive oxygen species-studies in white blood cells and in animal models, Antioxid. Redox Signal 20 (2014) 247–266.

[16] L.G. Bucciarelli, T. Wendt, W. Qu, Y. Lu, E. Lalla, L.L. Rong, M.T. Goova, B. Moser, T. Kislinger, D.C. Lee, Y. Kashyap, D.M. Stern, A.M. Schmidt, RAGE blockade stabilizes established atherosclerosis in diabetic apolipoprotein E-null mice, Circulation 106 (2002) 2827–2835.

[17] T. Rieg, T. Masuda, M. Gerasimova, E. Mayoux, K. Platt, D.R. Powell, S.C. Thomson, H. Koepsell, V. Vallon, Increase in SGLT1-mediated transport explains renal glucose reabsorption during genetic and pharmacological SGLT2 inhibition in euglycemia, American journal of physiology, *Am. J. Physiol. Renal Physiol.*306 (2014) F188–F193.

[18] M. Oelze, S. Kroller-Schon, P. Welschof, T. Jansen, M. Hausding, Y. Mikhed, P. Stamm, M. Mader, E. Zinssius, S. Agdauletova, A. Gottschlich, S. Steven, E. Schulz, S.P. Bottari, E. Mayoux, T. Munzel, A. Daiber, The sodium-glucose co-transporter 2 inhibitor empagliflozin improves diabetes-induced vascular dysfunction in the streptozotocin diabetes rat model by interfering with oxidative stress and glucotoxicity, PLoS One 9 (2014) e112394.

[19] A.J. Scheen, N. Paquot, Metabolic effects of SGLT-2 inhibitors beyond increased glucosuria: a review of the clinical evidence, Diabetes Metab. 40 (2014) S4–S11.

[20] J.L. Evans, I.D. Goldfine, Aging and insulin resistance: just say iNOS, Diabetes 62 (2013) 346–348.

[21] L. Fala, Jardiance (empagliflozin), an SGLT2 inhibitor, receives FDA approval for the treatment of patients with type 2, Diabetes, Am. Health Drug Benefits 8 (2015) 92–95.

[22] D. Fitchett, B. Zinman, C. Wanner, J.M. Lachin, S. Hantel, A. Salsali, O.E. Johansen, H.J. Woerle, U.C. Broedl, S.E. Inzucchi, E.-R. O. t. investigators, Heart failure outcomes with empagliflozin in patients with type 2 diabetes at high cardiovascular risk: results of the EMPA-REG OUTCOME(R) trial, Eur. Heart J. 37 (2016) 1526–1534.

[23] M.A. Pfeffer, B. Claggett, R. Diaz, K. Dickstein, H.C. Gerstein, L.V. Kober, F.C. Lawson, L. Ping, X. Wei, E.F. Lewis, A.P. Maggioni, J.J. McMurray, J.L. Probstfield, M.C. Riddle, S.D. Solomon, J.C. Tardif, E. Investigators, Lixisenatide in patients with type 2 diabetes and acute coronary syndrome, N. Engl. J. Med 373 (2015) 2247–2257.

[24] J.B. Green, M.A. Bethel, P.W. Armstrong, J.B. Buse, S.S. Engel, J. Garg, R. Josse, K.D. Kaufman, J. Koglin, S. Korn, J.M. Lachin, D.K. McGuire, M.J. Pencina, E. Standl, P.P. Stein, S. Suryawanshi, F. Van de Werf, E.D. Peterson, R.R. Holman, T.S. Group, Effect of sitagliptin on cardiovascular outcomes in type 2 diabetes, N. Engl. J. Med 373 (2015) 232–242.

[25] H.H. Hansen, J. Jelsing, C.F. Hansen, G. Hansen, N. Vrang, M. Mark, T. Klein, E. Mayoux, The sodium glucose cotransporter type 2 inhibitor empagliflozin preserves beta-cell mass and restores glucose homeostasis in the male zucker diabetic fatty rat, J. Pharmacol. Exp. Ther. 350 (2014) 657–664.

[26] S.P. Vickers, S.C. Cheetham, K.R. Headland, K. Dickinson, R. Grempler, E. Mayoux, M. Mark, T. Klein, Combination of the sodium-glucose cotransporter-2 inhibitor empagliflozin with orlistat or sibutramine further improves the body-weight reduction and glucose homeostasis of obese rats fed a cafeteria diet, Diabetes, Metab. Syndr. Obes.: Targets Ther. 7 (2014) 265–275.

[27] S.T. Cheng, L. Chen, S.Y. Li, E. Mayoux, P.S. Leung, The effects of empagliflozin, an SGLT2 inhibitor, on pancreatic beta-cell mass and glucose homeostasis in type 1 diabetes, PLoS One 11 (2016) e0147391.

[28] M. Oelze, S. Kröller-Schön, M. Mader, E. Zinßius, P. Stamm, M. Hausding, E. Mayoux, P. Wenzel, E. Schulz, T. Münzel, A. Daiber, Effects of empagliflozin on oxidative stress and endothelial dysfunction in STZ-induced Type 1 diabetic rat, Diabetol. Stoffwechs. 9 (2014) P247.

[29] P. Wenzel, E. Schulz, M. Oelze, J. Muller, S. Schuhmacher, M.S. Alhamdani, J. Debrezion, M. Hortmann, K. Reifenberg, I. Fleming, T. Munzel, A. Daiber, AT1-receptor blockade by telmisartan upregulates GTP-cyclohydrolase I and protects eNOS in diabetic rats, Free Radic. Biol. Med. 45 (2008) 619–626.

[30] S. Kroller-Schon, M. Knorr, M. Hausding, M. Oelze, A. Schuff, R. Schell, S. Sudowe, A. Scholz, S. Daub, S. Karbach, S. Kossmann, T. Gori, P. Wenzel, E. Schulz, S. Grabbe, T. Klein, T. Munzel, A. Daiber, Glucose-independent improvement of vascular dysfunction in experimental sepsis by dipeptidyl-peptidase 4 inhibition, Cardiovasc. Res. 96 (2012) 140–149.

[31] M. Oelze, A. Daiber, R.P. Brandes, M. Hortmann, P. Wenzel, U. Hink, E. Schulz, H. Mollnau, A. von Sandersleben, A.L. Kleschyov, A. Mulsch, H. Li, U. Forstermann, T. Munzel, Nebivolol inhibits superoxide formation by NADPH oxidase and endothelial dysfunction in angiotensin II-treated rats, Hypertension 48 (2006) 677–684.

[32] M. Oelze, M. Knorr, S. Schuhmacher, T. Heeren, C. Otto, E. Schulz, K. Reifenberg, P. Wenzel, T. Munzel, A. Daiber, Vascular dysfunction in streptozotocin-induced experimental diabetes strictly depends on insulin deficiency, J. Vasc. Res. 48 (2011) 275–284.

[33] M. Oelze, S. Kroller-Schon, S. Steven, E. Lubos, C. Doppler, M. Hausding, S. Tobias, C. Brochhausen, H. Li, M. Torzewski, P. Wenzel, M. Bachschmid, K.J. Lackner,

E. Schulz, T. Munzel, A. Daiber, Glutathione peroxidase-1 deficiency potentiates dysregulatory modifications of endothelial nitric oxide synthase and vascular dysfunction in aging, Hypertension 63 (2014) 390–396.
[34] M. McMichael, E. Hellstrom-Lindahl, H. Weiner, Identification and selective precipitation of human aldehyde dehydrogenase isozymes using antibodies raised to horse liver aldehyde dehydrogenase isozymes, Alcohol., Clin. Exp. Res. 10 (1986) 323–329.
[35] M. Hausding, K. Jurk, S. Daub, S. Kroller-Schon, J. Stein, M. Schwenk, M. Oelze, Y. Mikhed, J.G. Kerahrodi, S. Kossmann, T. Jansen, E. Schulz, P. Wenzel, A.B. Reske-Kunz, C. Becker, T. Munzel, S. Grabbe, A. Daiber, CD40L contributes to angiotensin II-induced pro-thrombotic state, vascular inflammation, oxidative stress and endothelial dysfunction, Basic Res Cardiol. 108 (2013) 386.
[36] D. Umlauf, Y. Goto, R. Feil, Site-specific analysis of histone methylation and acetylation, Methods Mol. Biol. 287 (2004) 99–120.
[37] C. Cosseau, C. Grunau, Native chromatin immunoprecipitation, Methods Mol. Biol. 791 (2011) 195–212.
[38] Z. Wu, D. Siuda, N. Xia, G. Reifenberg, A. Daiber, T. Munzel, U. Forstermann, H. Li, Maternal treatment of spontaneously hypertensive rats with pentaerythritol tetranitrate reduces blood pressure in female offspring, Hypertension 65 (2015) 232–237.
[39] H. Li, P. Junk, A. Huwiler, C. Burkhardt, T. Wallerath, J. Pfeilschifter, U. Forstermann, Dual effect of ceramide on human endothelial cells: induction of oxidative stress and transcriptional upregulation of endothelial nitric oxide synthase, Circulation 106 (2002) 2250–2256.
[40] M.I. Lin, D. Fulton, R. Babbitt, I. Fleming, R. Busse, K.A. Pritchard Jr, W.C. Sessa, Phosphorylation of threonine 497 in endothelial nitric-oxide synthase coordinates the coupling of L-arginine metabolism to efficient nitric oxide production, J. Biol. Chem. 278 (2003) 44719–44726.
[41] I. Fleming, B. Fisslthaler, S. Dimmeler, B.E. Kemp, R. Busse, Phosphorylation of Thr (495) regulates Ca(2+)/calmodulin-dependent endothelial nitric oxide synthase activity, Circ. Res. 88 (2001) E68–E75.
[42] L. Chen, T. Klein, P.S. Leung, Effects of combining linagliptin treatment with BI-38335, a novel SGLT2 inhibitor, on pancreatic islet function and inflammation in db/db mice, Curr. Mol. Med. 12 (2012) 995–1004.
[43] N. Terami, D. Ogawa, H. Tachibana, T. Hatanaka, J. Wada, A. Nakatsuka, J. Eguchi, C.S. Horiguchi, N. Nishii, H. Yamada, K. Takei, H. Makino, Long-term treatment with the sodium glucose cotransporter 2 inhibitor, dapagliflozin, ameliorates glucose homeostasis and diabetic nephropathy in db/db mice, PLoS One 9 (2014) e100777.
[44] Y. Tokuyama, J. Sturis, A.M. DePaoli, J. Takeda, M. Stoffel, J. Tang, X. Sun, K.S. Polonsky, G.I. Bell, Evolution of beta-cell dysfunction in the male Zucker diabetic fatty rat, Diabetes 44 (1995) 1447–1457.
[45] M. Prentki, C.J. Nolan, Islet beta cell failure in type 2 diabetes, J. Clin. Investig. 116 (2006) 1802–1812.
[46] C. Kuriyama, J.Z. Xu, S.P. Lee, J. Qi, H. Kimata, T. Kakimoto, K. Nakayama, Y. Watanabe, N. Taniuchi, K. Hikida, Y. Matsushita, K. Arakawa, A. Saito, K. Ueta, M. Shiotani, Analysis of the effect of canagliflozin on renal glucose reabsorption and progression of hyperglycemia in zucker diabetic Fatty rats, J. Pharmacol. Exp. Ther. 351 (2014) 423–431.
[47] Y. Liang, K. Arakawa, K. Ueta, Y. Matsushita, C. Kuriyama, T. Martin, F. Du, Y. Liu, J. Xu, B. Conway, J. Conway, D. Polidori, K. Ways, K. Demarest, Effect of canagliflozin on renal threshold for glucose, glycemia, and body weight in normal and diabetic animal models, PLoS One 7 (2012) e30555.
[48] Y. Watanabe, K. Nakayama, N. Taniuchi, Y. Horai, C. Kuriyama, K. Ueta, K. Arakawa, T. Senbonmatsu, M. Shiotani, Beneficial effects of canagliflozin in combination with pioglitazone on insulin sensitivity in rodent models of obese type 2 diabetes, PLoS One 10 (2015) e0116851.
[49] B. Lin, N. Koibuchi, Y. Hasegawa, D. Sueta, K. Toyama, K. Uekawa, M. Ma, T. Nakagawa, H. Kusaka, S. Kim-Mitsuyama, Glycemic control with empagliflozin, a novel selective SGLT2 inhibitor, ameliorates cardiovascular injury and cognitive dysfunction in obese and type 2 diabetic mice, Cardiovasc. Diabetol. 13 (2014) 148.
[50] G. Luippold, T. Klein, M. Mark, R. Grempler, Empagliflozin, a novel potent and selective SGLT-2 inhibitor, improves glycaemic control alone and in combination with insulin in streptozotocin-induced diabetic rats, a model of type 1 diabetes mellitus, Diabetes, Obes. Metab. 14 (2012) 601–607.
[51] B.A. Perkins, D.Z. Cherney, H. Partridge, N. Soleymanlou, H. Tschirhart, B. Zinman, N.M. Fagan, S. Kaspers, H.J. Woerle, U.C. Broedl, O.E. Johansen, Sodium-glucose cotransporter 2 inhibition and glycemic control in type 1 diabetes: results of an 8-week open-label proof-of-concept trial, Diabetes Care 37 (2014) 1480–1483.
[52] D.Z. Cherney, B.A. Perkins, N. Soleymanlou, R. Har, N. Fagan, O.E. Johansen, H.J. Woerle, M. von Eynatten, U.C. Broedl, The effect of empagliflozin on arterial stiffness and heart rate variability in subjects with uncomplicated type 1 diabetes mellitus, Cardiovasc. Diabetol. 13 (2014) 28.
[53] A. Bierhaus, T. Fleming, S. Stoyanov, A. Leffler, A. Babes, C. Neacsu, S.K. Sauer, M. Eberhardt, M. Schnolzer, F. Lasitschka, W.L. Neuhuber, T.I. Kichko, I. Konrade, R. Elvert, W. Mier, V. Pirags, I.K. Lukic, M. Morcos, T. Dehmer, N. Rabbani, P.J. Thornalley, D. Edelstein, C. Nau, J. Forbes, P.M. Humpert, M. Schwaninger, D. Ziegler, D.M. Stern, M.E. Cooper, U. Haberkorn, M. Brownlee, P.W. Reeh, P.P. Nawroth, Methylglyoxal modification of Nav1.8 facilitates nociceptive neuron firing and causes hyperalgesia in diabetic neuropathy, Nat. Med 18 (2012) 926–933.
[54] M. Sun, M. Yokoyama, T. Ishiwata, G. Asano, Deposition of advanced glycation end products (age) and expression of the receptor for age in cardiovascular tissue of the diabetic rat, Int. J. Exp. Pathol. 79 (1998) 207–222.
[55] J.L. Wautier, M.P. Wautier, A.M. Schmidt, G.M. Anderson, O. Hori, C. Zoukourian, L. Capron, O. Chappey, S.D. Yan, J. Brett, et al., Advanced glycation end products (AGEs) on the surface of diabetic erythrocytes bind to the vessel wall via a specific receptor inducing oxidant stress in the vasculature: a link between surface-associated AGEs and diabetic complications, Proc. Natl. Acad. Sci. USA 91 (1994) 7742–7746.
[56] A. Daiber, S. Steven, A. Weber, V.V. Shuvaev, V.R. Muzykantov, I. Laher, H. Li, S. Lamas, T. Munzel, Targeting vascular (endothelial) dysfunction, Br. J. Pharmacol. 174 (2017) 1591–1619.
[57] A. Daiber, F. Di Lisa, M. Oelze, S. Kroller-Schon, S. Steven, E. Schulz, T. Munzel, Crosstalk of mitochondria with NADPH oxidase via reactive oxygen and nitrogen species signalling and its role for vascular function, Br. J. Pharmacol. 174 (2017) 1670–1689.
[58] Y. Tekabe, T. Anthony, Q. Li, R. Ray, V. Rai, G. Zhang, A.M. Schmidt, L.L. Johnson, Treatment effect with anti-RAGE F(ab')2 antibody improves hind limb angiogenesis and blood flow in Type 1 diabetic mice with left femoral artery ligation, Vasc. Med. 20 (2015) 212–218.
[59] M.B. Grauballe, J.A. Ostergaard, S. Schou, A. Flyvbjerg, P. Holmstrup, Blockade of RAGE in Zucker obese rats with experimental periodontitis, J. Periodontal Res. (2016).
[60] V. Vallon, M. Gerasimova, M.A. Rose, T. Masuda, J. Satriano, E. Mayoux, H. Koepsell, S.C. Thomson, T. Rieg, SGLT2 inhibitor empagliflozin reduces renal growth and albuminuria in proportion to hyperglycemia and prevents glomerular hyperfiltration in diabetic Akita mice, American journal of physiology, Ren. Physiol. 306 (2014) F194–F204.
[61] F. Gembardt, C. Bartaun, N. Jarzebska, E. Mayoux, V.T. Todorov, B. Hohenstein, C. Hugo, The SGLT2 inhibitor empagliflozin ameliorates early features of diabetic nephropathy in BTBR ob/ob type 2 diabetic mice with and without hypertension, Am. J. physiol. Ren. Physiol. 307 (2014) F317–F325.
[62] M. Bassirat, Z. Khalil, Short- and long-term modulation of microvascular responses in streptozotocin-induced diabetic rats by glycosylated products, J. Diabetes Complicat. 24 (2010) 64–72.
[63] J.H. Han, T.J. Oh, G. Lee, H.J. Maeng, D.H. Lee, K.M. Kim, S.H. Choi, H.C. Jang, H.S. Lee, K.S. Park, Y.B. Kim, S. Lim, The beneficial effects of empagliflozin, an SGLT2 inhibitor, on atherosclerosis in ApoE -/- mice fed a western diet, Diabetologia (2016).
[64] L. Thomas, M. Tadayyon, M. Mark, Chronic treatment with the dipeptidyl peptidase-4 inhibitor BI 1356 [(R)−8-(3-amino-piperidin-1-yl)−7-but-2-ynyl-3-methyl-1-(4-methyl-quinazol in-2-ylmethyl)−3,7-dihydro-purine-2,6-dione] increases basal glucagon-like peptide-1 and improves glycemic control in diabetic rodent models, J. Pharmacol. Exp. Ther. 328 (2009) 556–563.
[65] L. Ferreira, E. Teixeira-de-Lemos, F. Pinto, B. Parada, C. Mega, H. Vala, R. Pinto, P. Garrido, J. Sereno, R. Fernandes, P. Santos, I. Velada, A. Melo, S. Nunes, F. Teixeira, F. Reis, Effects of sitagliptin treatment on dysmetabolism, inflammation, and oxidative stress in an animal model of type 2 diabetes (ZDF rat), Mediat. Inflamm. 2010 (2010) 592760.
[66] N. Apaijai, H. Pintana, S.C. Chattipakorn, N. Chattipakorn, Effects of vildagliptin versus sitagliptin, on cardiac function, heart rate variability and mitochondrial function in obese insulin-resistant rats, Br. J. Pharmacol. 169 (2013) 1048–1057.
[67] N. Yokoi, M. Hoshino, S. Hidaka, E. Yoshida, M. Beppu, R. Hoshikawa, K. Sudo, A. Kawada, S. Takagi, S. Seino, A novel rat model of type 2 diabetes: the Zucker fatty diabetes mellitus ZFDM rat, J. Diabetes Res. 2013 (2013) 103731.
[68] J. Bolinder, O. Ljunggren, J. Kullberg, L. Johansson, J. Wilding, A.M. Langkilde, J. Sugg, S. Parikh, Effects of dapagliflozin on body weight, total fat mass, and regional adipose tissue distribution in patients with type 2 diabetes mellitus with inadequate glycemic control on metformin, J. Clin. Endocrinol. Metab. 97 (2012) 1020–1031.
[69] Z. Chen, J. Zhang, J.S. Stamler, Identification of the enzymatic mechanism of nitroglycerin bioactivation, Proc. Natl. Acad. Sci. USA 99 (2002) 8306–8311.
[70] K. Sydow, A. Daiber, M. Oelze, Z. Chen, M. August, M. Wendt, V. Ullrich, A. Mulsch, E. Schulz, J.F. Keaney Jr., J.S. Stamler, T. Munzel, Central role of mitochondrial aldehyde dehydrogenase and reactive oxygen species in nitroglycerin tolerance and cross-tolerance, J. Clin. Investig. 113 (2004) 482–489.
[71] P. Wenzel, U. Hink, M. Oelze, S. Schuppan, K. Schaeuble, S. Schildknecht, K.K. Ho, H. Weiner, M. Bachschmid, T. Munzel, A. Daiber, Role of reduced lipoic acid in the redox regulation of mitochondrial aldehyde dehydrogenase (ALDH-2) activity. Implications for mitochondrial oxidative stress and nitrate tolerance, J. Biol. Chem. 282 (2007) 792–799.
[72] C.H. Chen, G.R. Budas, E.N. Churchill, M.H. Disatnik, T.D. Hurley, D. Mochly-Rosen, Activation of aldehyde dehydrogenase-2 reduces ischemic damage to the heart, Science 321 (2008) 1493–1495.
[73] J. Wang, H. Wang, P. Hao, L. Xue, S. Wei, Y. Zhang, Y. Chen, Inhibition of aldehyde dehydrogenase 2 by oxidative stress is associated with cardiac dysfunction in diabetic rats, Mol. Med. 17 (2011) 172–179.
[74] P. Wenzel, S. Schuhmacher, J. Kienhofer, J. Muller, M. Hortmann, M. Oelze, E. Schulz, N. Treiber, T. Kawamoto, K. Scharffetter-Kochanek, T. Munzel, A. Burkle, M.M. Bachschmid, A. Daiber, Manganese superoxide dismutase and aldehyde dehydrogenase deficiency increase mitochondrial oxidative stress and aggravate age-dependent vascular dysfunction, Cardiovasc. Res. 80 (2008) 280–289.
[75] M. Brandt, V. Garlapati, M. Oelze, E. Sotiriou, M. Knorr, S. Kroller-Schon, S. Kossmann, T. Schonfelder, H. Morawietz, E. Schulz, H.P. Schultheiss, A. Daiber, T. Munzel, P. Wenzel, NOX2 amplifies acetaldehyde-mediated cardiomyocyte mitochondrial dysfunction in alcoholic cardiomyopathy, Sci. Rep. 6 (2016) 32554.
[76] P. Wenzel, J. Muller, S. Zurmeyer, S. Schuhmacher, E. Schulz, M. Oelze, A. Pautz, T. Kawamoto, L. Wojnowski, H. Kleinert, T. Munzel, A. Daiber, ALDH-2 deficiency increases cardiovascular oxidative stress–evidence for indirect antioxidative properties, Biochem Biophys. Res. Commun. 367 (2008) 137–143.
[77] G. Wolkart, M. Beretta, M.V. Wenzl, H. Stessel, K. Schmidt, N. Maeda, B. Mayer,

A. Schrammel, Tolerance to nitroglycerin through proteasomal down-regulation of aldehyde dehydrogenase-2 in a genetic mouse model of ascorbate deficiency, Br. J. Pharmacol. 168 (2013) 1868–1877.
[78] K. Srinivasan, P. Ramarao, Animal models in type 2 diabetes research: an overview, Indian J. Med. Res. 125 (2007) 451–472.
[79] A. Ojima, T. Matsui, Y. Nishino, N. Nakamura, S. Yamagishi, Empagliflozin, an inhibitor of sodium-glucose cotransporter 2 exerts anti-inflammatory and anti-fibrotic effects on experimental diabetic nephropathy partly by suppressing AGEs-receptor axis, Horm. Metab. Res. 47 (2015) 686–692.
[80] T. Heise, E. Seewaldt-Becker, S. Macha, S. Hantel, S. Pinnetti, L. Seman, H.J. Woerle, Safety, tolerability, pharmacokinetics and pharmacodynamics following 4 weeks' treatment with empagliflozin once daily in patients with type 2 diabetes, Diabetes, Obes. Metab. 15 (2013) 613–621.
[81] S.A. Hawley, R.J. Ford, B.K. Smith, G.J. Gowans, S.J. Mancini, R.D. Pitt, E.A. Day, I.P. Salt, G.R. Steinberg, D.G. Hardie, The Na+/Glucose Cotransporter Inhibitor Canagliflozin Activates AMPK by inhibiting mitochondrial function and increasing cellular AMP levels, Diabetes 65 (2016) 2784–2794.
[82] C. Bonner, J. Kerr-Conte, V. Gmyr, G. Queniat, E. Moerman, J. Thevenet, C. Beaucamps, N. Delalleau, I. Popescu, W.J. Malaisse, A. Sener, B. Deprez, A. Abderrahmani, B. Staels, F. Pattou, Inhibition of the glucose transporter SGLT2 with dapagliflozin in pancreatic alpha cells triggers glucagon secretion, Nat. Med. 21 (2015) 512–517.
[83] A. Jufvas, S. Sjodin, K. Lundqvist, R. Amin, A.V. Vener, P. Stralfors, Global differences in specific histone H3 methylation are associated with overweight and type 2 diabetes, Clin. Epigenetics 5 (2013) 15.
[84] F. Miao, D.D. Smith, L. Zhang, A. Min, W. Feng, R. Natarajan, Lymphocytes from patients with type 1 diabetes display a distinct profile of chromatin histone H3 lysine 9 dimethylation: an epigenetic study in diabetes, Diabetes 57 (2008) 3189–3198.